Available online at www.sciencedirect.com
ScienceDirect
Journal of Theoretical Biology 249 (2007) 29–45
Journal of Theoretical Biology
www.elsevier.com/locate/yjtbi

Rhythms of high-grade block in an ionic model of a strand of regionally ischemic ventricular muscle

Alejandro López[a], Humberto Arce[a], Michael R. Guevara[b,*]

[a]*Departamento de Física, Facultad de Ciencias, Universidad Nacional Autónoma de México, Apartado Postal 70-542, 04510 México, Distrito Federal, México*
[b]*Department of Physiology and Centre for Nonlinear Dynamics in Physiology and Medicine, McGill University, 3655 Sir William Osler Promenade, Montréal, Québec, Canada H3G 1Y6*

Received 21 July 2006; received in revised form 11 June 2007; accepted 11 June 2007
Available online 21 June 2007

Abstract

Electrical alternans, a beat-to-beat alternation in the electrocardiogram or electrogram, is frequently seen during the first few minutes of acute myocardial ischemia, and is often immediately followed by malignant cardiac arrhythmias such as ventricular tachycardia and ventricular fibrillation. As ischemia progresses, higher-order periodic rhythms (e.g., period-4) can replace the period-2 alternans rhythm. This is also seen in modelling work on a two-dimensional (2-D) sheet of regionally ischemic ventricular muscle. In addition, in the experimental work, ventricular arrhythmias are overwhelmingly seen only after the higher-order rhythms arise. We investigate an ionic model of a strand of ischemic ventricular muscle, constructed as a 3-cm-long 1-D cable with a centrally located 1-cm-long segment exposed to an elevated extracellular potassium concentration ($[K^+]_o$). As $[K^+]_o$ is raised in this "ischemic segment" to represent one major effect of ongoing ischemia, the sequence of rhythms {1:1 → 2:2 (alternans) → 2:1} is seen. With further increase in $[K^+]_o$, one sees higher-order periodic $2N$:M rhythms {2:1 → 4:2 → 4:1 → 6:2 → 6:1 → 8:2 → 8:1}. In a $2N$:M cycle, only M of the $2N$ action potentials generated at the proximal end of the cable successfully traverse the ischemic segment, with the remaining ones being blocked within the ischemic segment. Finally, there is a transition to complete block {8:1 → 2:0 → 1:0} (in an n:0 rhythm, all action potentials die out within the ischemic segment). Changing the length of the ischemic segment results in different rhythms and transitions being seen: e.g., when the ischemic segment is 2 cm long, the period-6 rhythms are not seen; when it is 0.5 cm long, there is a 3:1 rhythm interposed between the 2:1 and 1:0 rhythms. We discuss the relevance of our results to the experimental observations on the higher-order rhythms that presage reentrant ischemic ventricular arrhythmias.

Keywords: Period multupling; Alternans; Bifurcations; Ventricular arrhythmias; Conduction block

1. Introduction

Reentrant arrhythmias such as ventricular tachycardia and ventricular fibrillation often occur during myocardial ischemia. It is often observed that the normal 1:1 activation sequence of the heart is disrupted before these arrhythmias start. There can be an alternans or 2:2 rhythm, in which there is a beat-to-beat alternation in some characteristic feature of the recording, e.g., the T-wave in the electrocardiogram or electrogram, the duration of the action potential in an intracellular recording. There can be 2:1 block, in which every second action potential stops propagating ("blocks") somewhere within the ischemic area. There are in fact dozens of experimental reports showing that these two period-2 rhythms exist seconds or minutes before malignant arrhythmias are initiated (e.g., Scherlag et al., 1974; Downar et al., 1977; Russell et al., 1979; Cinca et al., 1980; Janse et al., 1980; Hashimoto et al., 1984; Carson et al., 1986; Dilly and Lab, 1988; Abe et al., 1989; Konta et al., 1990; Nearing et al., 1991; Tachibana et al., 1998; Nearing and Verrier, 2002, 2003).

*Corresponding author. Tel.: +1 514 398 4320; fax: +1 514 398 7452.
E-mail addresses: allv@hp.fciencias.unam.mx (A. López), jhar@hp.fciencias.unam.mx (H. Arce), michael.guevara@mcgill.ca (M.R. Guevara).

0022-5193/$ - see front matter © 2007 Elsevier Ltd. All rights reserved.
doi:10.1016/j.jtbi.2007.06.015

In contrast, with one exception, there have been only a few scattered incidental reports of higher-order "period-multupled" rhythms (e.g., period-3 and period-4 rhythms, in which it takes 3 or 4 beats for the rhythm to recur) in the acutely ischemic ventricle (Russell et al., 1979; Hashimoto et al., 1984; Dilly and Lab, 1988; Laguna et al., 1999; Wu and Zipes, 2001). In the only systematic experimental study to date (Nearing and Verrier, 2002), these higher-order rhythms always arose immediately out of a phase of alternans rhythm as the ischemia progressed. Six of the 12 dogs studied eventually went on to fibrillate, and higher-order rhythms were followed in five of these six dogs within a few tens of seconds by more complex rhythms and ventricular fibrillation, with the remaining dog going directly from high-amplitude alternans to fibrillation. In the six dogs that did not fibrillate, higher-order rhythms were not seen; alternans was seen in four of these six animals, and in two of these four animals, the alternans was at very low amplitude (see Figs. 2 and 3 of Nearing and Verrier, 2002).

The electrophysiological disturbances during ischemia are caused by many factors (Wit and Janse, 1993; Carmeliet, 1999). Perhaps chief among these is a rise in external potassium concentration ($[K^+]_o$). We have thus modelled the regionally ischemic ventricle by increasing $[K^+]_o$ within a circumscribed area (the ischemic zone) lying within the interior of a 2-D sheet of ventricular muscle (Xu and Guevara, 1998; Arce et al., 2000). Reentrant arrhythmias of the spiral-wave type occur in this model in response to incremental pacing at a fixed elevated $[K^+]_o$ (Xu and Guevara (1998); see also Bernus et al. (2005) for a more recent 3-D simulation). When $[K^+]_o$ is incrementally raised at a fixed pacing cycle length to simulate the natural progression of events during acute ischemia, 1:1 rhythm is replaced in turn by 2:2 rhythm, 2:1 block, various higher-order rhythms (e.g., 4:1 block), and eventually complete block (Arce et al., 2000). We have also made a detailed modelling study of the manner in which period-2 rhythms arise in the simpler case of a 1-D strand of ventricular muscle containing a central segment with elevated $[K^+]_o$ (Arce et al., 2002). Since 4:1 block and other higher-order rhythms were seen in the earlier work on the 2-D sheet (Arce et al., 2000), we decided to carry out a more systematic study of these higher-order rhythms of block in the model of a 1-D strand of regionally ischemic ventricular muscle.

2. Methods

We study an ionic model of a 1-D strand of normal ventricular myocardium, with an area of elevated $[K^+]_o$ within its centre (the "ischemic segment") to represent the ischemic zone (Tilg and Wach, 1995; Ferrero et al., 1997; Cimponeriu et al., 1998; Xu and Guevara, 1998; Feldman et al., 1999; Arce et al., 2000, 2002; Wang and Rudy, 2000). We continue to use a simple "first-generation" model of the ionic currents rather than one of the several more complex "second-generation" models incorporating the Na^+–K^+ pump current and the Na^+–Ca^{2+} exchange current that are presently available, due to the fact that in their original formulation, second-generation models have two attributes: (i) degeneracy, with non-uniqueness of equilibria such as steady states and limit cycles, and (ii) very slow long-term drifts in the variables (further discussion of these complicating factors can be found in Krogh-Madsen et al. (2005)). As in other recent studies, one can avoid both of these characteristics either by continuing to use an explicitly first-generation model (ten Tusscher and Panfilov, 2003) or by using a second-generation model that is rendered essentially first-generation by keeping internal ionic concentrations constant (Bernus et al., 2002). We take the first of these approaches, selecting the Luo–Rudy (LR) model because it has $[K^+]_o$ as a parameter, which is essential for our modelling of the ischemic segment (Luo and Rudy, 1991).

One deficiency of the space-clamped LR model, which is carried over from the Beeler–Reuter model from which it is derived (Beeler and Reuter, 1977), is that the time-constants for the activation and inactivation of the slow inward Ca^{2+} current (I_{si}) are both an order of magnitude too large with respect to the experimental values. We have thus decreased the time constant for the activation of I_{si} (τ_d) by a factor of 10, which then puts τ_d into the physiologic range (Isenberg and Klöckner, 1982; Xu and Guevara, 1998). As in our prior work on modelling alternans in ischemic muscle (Arce et al., 2000, 2002), we leave the inactivation time-constant of I_{si} (τ_f) unchanged, since reducing it results in the level of the plateau of the action potential being too depressed. In addition, leaving τ_f unchanged results in a long-lasting I_{si} waveform that is very similar to that seen in the action-potential-clamp current trace when Ca^{2+}-entry is blocked in experiments on ventricular cells (Linz and Meyer, 2000).

We use the equations appearing in Table 1 and in the body of the text of Luo and Rudy (1991). The ionic concentrations given there are used to calculate the reversal potentials E_{Na}, E_K, E_{Kp}, and E_{K1}. Using the equations in Table 1 of Luo and Rudy (1991) results in current–voltage relationships for I_{K1} and $I_{K1(T)}$ that are different from those shown in Figs. 2 and 3B, respectively, of that paper. Nevertheless, using those equations (i.e., with unmodified τ_d), and starting from infinite-rest initial conditions at the nominal $[K^+]_o$ of 5.4 mM, we obtain an action potential that superimposes with that shown in Fig. 4A of Luo and Rudy (1991). A full listing of the equations of our modified model is given in Supplementary Material I. In the steady state, the action potential duration (measured between the upstroke and the crossing through of −60 mV on the repolarizing limb of the action potential) is reduced to ~237 ms from ~290 ms in the standard LR space-clamped model when paced at a basic cycle length (BCL) of 400 ms.

We model a 1-D strand of muscle by the 1-D cable equation

$$\partial^2 V/\partial x^2 = \rho S_v(C_m \partial V/\partial t + I_{ion}), \quad (1)$$

where V is the transmembrane potential (mV), x is the spatial coordinate in the strand (cm), ρ is the effective longitudinal resistivity (0.2 kΩ-cm), S_v is the surface-to-volume ratio (5000 cm^{-1}), C_m is the specific membrane capacitance (1 μF cm^{-2}), t is time (ms), and I_{ion} is the total ionic current (μA cm^{-2}) given by our modified LR model (Sharp and Joyner, 1980). We numerically integrate Eq. (1) using a central difference approximation for $\partial^2 V/\partial x^2$ and a forward difference approximation for $\partial V/\partial t$

$$[V_{i-1}(t) - 2V_i(t) + V_{i+1}(t)]/\Delta x^2 = \rho S_v\{C_m[V_i(t+\Delta t) - V_i(t)]/\Delta t + I_{ion,i}(t)\}, \quad (2)$$

where V_i is the voltage of the ith element in the cable, $I_{ion,i}$ is the ionic current in that element, Δx is the spatial step-size (0.01 cm), and Δt is the temporal step-size (0.01 ms). Each activation or inactivation variable ξ_j is calculated from

$$\xi_j(t+\Delta t) = \xi_{j\infty} - [\xi_{j\infty} - \xi_j(t)]\, e^{-\Delta t/\tau_j}, \quad (3)$$

where $\xi_{j\infty}$ is the steady state or asymptotic value of ξ_j and τ_j is the time constant of ξ_j, both of which are functions of V. A look-up table with linear interpolation (voltage-step = 0.2 mV) is used to calculate $\xi_{j\infty}$ and τ_j. The internal calcium concentration $[Ca^{2+}]_i$ is obtained from

$$[Ca^{2+}]_i(t+\Delta t) = [Ca^{2+}]_i(t) + \{d[Ca^{2+}]_i(t)/dt\}\,\Delta t. \quad (4)$$

The 1-D space-constant (λ) is $(R_m/\rho S_v)^{1/2} \cong 0.06$ cm, where R_m is the specific membrane resistance (3.55 kΩ-cm^2 at the nominal LR value of $[K^+]_o$ of 5.4 mM). The discretization factor ($\Delta x/\lambda$) is thus ~0.17, at which point the numerical error is acceptable (see Fig. 1 of Arce et al., 2002). The diffusion constant $D = 1/(\rho S_v C_m) = 10^{-3}$ cm^2 ms^{-1}, so that the von Neumann linear stability criterion ($(\Delta x)^2/\Delta t > 4D$) is satisfied. Sealed-end (i.e., zero-current flux) Neumann boundary conditions (i.e., $\partial V/\partial x = 0$) are set at both ends of the cable. Stimulation is carried out by injecting a 1 ms duration current pulse into the first five elements of the strand at an amplitude of 100 μA cm^{-2} (~2 × threshold).

An implicit integration scheme (Crank–Nicholson) was used to spot-check the results given below; the findings were similar, but with a small shift in the exact value of $[K^+]_o$ at which a particular rhythm is seen. The simulations below were carried out using programs written in C (~16 significant decimal places). Movies of propagation down the cable (Supplementary Material III) were made by generating a GIF picture showing the voltage as a function of position every 10 ms and then assembling these picture files into QuickTime movie (.mov) files.

3. Results

As ischemia progresses, there is a gradual increase in $[K^+]_o$ and in the size of the ischemic zone. We now explore the effect of increasing $[K^+]_o$ in the central part of the strand (the "ischemic segment") at a fixed BCL of 400 ms, but with the length of the ischemic segment kept fixed. We choose this BCL since it is at the center of the 300–500 ms range typically used in experimental work on ischemic arrhythmias (see Arce et al., 2000 for references). We first explore the case where the region of elevated $[K^+]_o$ occupies the central 1-cm portion of the strand, flanked on either side by a 1-cm segment of normal tissue (Arce et al., 2000, 2002). We then explore what happens when the length of the ischemic segment is different from 1 cm.

At the start of each simulation run at a new $[K^+]_o$, we obtain approximate infinite-rest initial conditions by setting the variables in the normal- and high-potassium regions equal to their respective space-clamped steady-state values and then allowing the simulation to run for 1000 ms so as to allow some time for equilibration to occur, before injecting the first stimulus at $t = 0$ ms. We inject at least 40 stimuli to allow transients due to initial conditions to dissipate. We now describe the sequence of rhythms seen as $[K^+]_o$ is raised.

3.1. Period-1 rhythm

Fig. 1A shows the transmembrane potential (V) as a function of time (t) at several points (x) along the 3-cm-long cable at $[K^+]_o = 5.4$ mM, i.e., in control conditions before $[K^+]_o$ is raised within the ischemic segment. In the steady state there is a 1:1 rhythm, in which each stimulus produces an action potential that travels down the cable with an invariant morphology. A periodic N:M rhythm exists at a given point in the cable when for every N stimuli there are M action potentials seen at that point. The overall response of the cable is described as an N:M rhythm when for every N action potentials in the most proximal segment there are M action potentials in the most distal segment. Fig. 1B shows that the resting membrane potential (RMP) and V_{max} (the maximum voltage achieved during one pacing cycle, which in this case corresponds to the overshoot potential of the action potential) do not change with distance x, provided that one is far enough away from the ends of the cable to avoid edge-effects. Such edge-effects are expected over a distance on the order of a few space constants ($\lambda = 0.6$ mm), and are in fact appreciable over a distance of ~1.5 mm, corresponding to 15 elements of the discretized cable. Fig. 1C gives the classic ladder diagram or laddergram, which plots the position of the upstroke of the action potential (arbitrarily defined here as the crossing of −40 mV) as a function of time, at a sampling interval of 2 ms. The reciprocal of the slope of this line is the conduction velocity, which is constant down the cable at ~60 cm s^{-1} (Arce et al., 2002).

When $[K^+]_o$ within the 1-cm-long ischemic segment is raised, but to a level that is not too high, the 1:1 rhythm persists. Fig. 1D–F shows that for $[K^+]_o = 13$ mM, as the action potential propagates into the ischemic segment, the RMP depolarizes to about −65 mV and V_{max} falls, so that there is a large decrease in action potential amplitude (difference between V_{max} and RMP). The action potential duration (APD) also falls (Fig. 1D), there is a decrease in

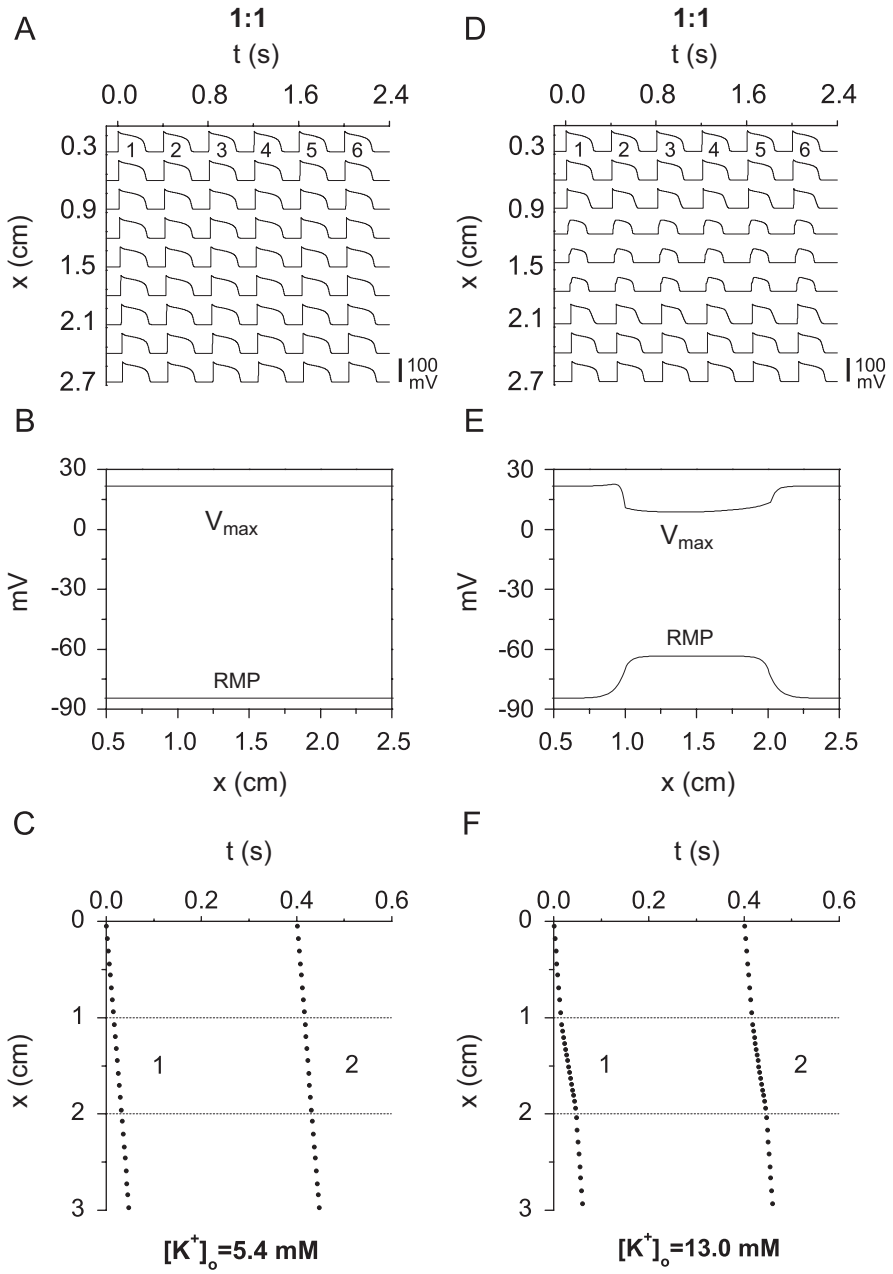

Fig. 1. *Period-1 rhythm*: 1:1 rhythm. External potassium concentration ($[K^+]_o$) = 5.4 mM (A–C); 13.0 mM (D–F). Length of ischemic segment = 1 cm. (A, C) Transmembrane potential as a function of time (t) at selected points spaced at a distance (x) of 0.3 cm on the cable. About 40 stimuli were injected just before the start of these traces. (B, E) The maximum voltage of the action potential (V_{max}) and the resting membrane potential (*RMP*) plotted as a function of distance (x) down the cable. (C, F) Laddergram, showing position of action potential upstroke in the cable as a function of time. A data-point is plotted every 2 ms.

the conduction velocity (Fig. 1F), and a two-component upstroke appears (Fig. 1D, but seen much more clearly in Fig. 2A of Arce et al., 2000). Similar results have been seen in experimental work (e.g., Scherlag et al., 1974; Downar et al., 1977; Russell et al., 1979; Cinca et al., 1980; Hashimoto et al., 1984; Carson et al., 1986; Abe et al., 1989; Koller et al., 2000; Wu and Zipes, 2001) and in earlier modelling work (Ferrero et al., 1997, 2003; Shaw and Rudy, 1997; Arce et al., 2000). Note that while the action potential decrements in amplitude as it enters the ischemic segment, it increments as it leaves (Fig. 1D and E). One can appreciate from the laddergram (Fig. 1F) that there is a significant slowing of conduction within the ischemic segment, both from the change in the slope of the line and the denser packing of data-points within the ischemic segment. Movies showing the action potential spreading down the strand for Fig. 1 and the other figures below are available as Supplementary Material III on the journal web-site (and also at: http://www.medicine.mcgill.ca/physio/guevaralab/arce-III.htm).

3.2. Period-2 rhythms

As $[K^+]_o$ is increased to just above ~13.170 mM, the 1:1 rhythm is lost and is replaced with a 2:2 or alternans rhythm (Fig. 2A: $[K^+]_o = 13.173$ mM). The basic repeating cycle of this rhythm consists of two different action potentials, both of which are full-sized provided that the recording site is far enough away from the distal part of the ischemic segment (Fig. 2A). Fig. 2B gives V_{max} for the odd- and even-numbered beats as a function of distance: as the action potential enters the ischemic segment, every second action potential (even-numbered beats in Fig. 2A) decrements to the point where it becomes very small in amplitude within the distal part of the ischemic segment (Fig. 2A). Note that while the even-numbered action potentials in Fig. 2A decrement sharply within the first half of the ischemic segment, they attain a more-or-less constant V_{max} within the distal portion of the ischemic segment, before incrementing back up to full-sized action potentials as they leave the ischemic segment (*beat 2* in Fig. 2B). We have previously termed this propagating response the "maintained small-amplitude response" (Arce et al., 2000, 2002). Since the maintained small-amplitude response travels more slowly than the full-sized action

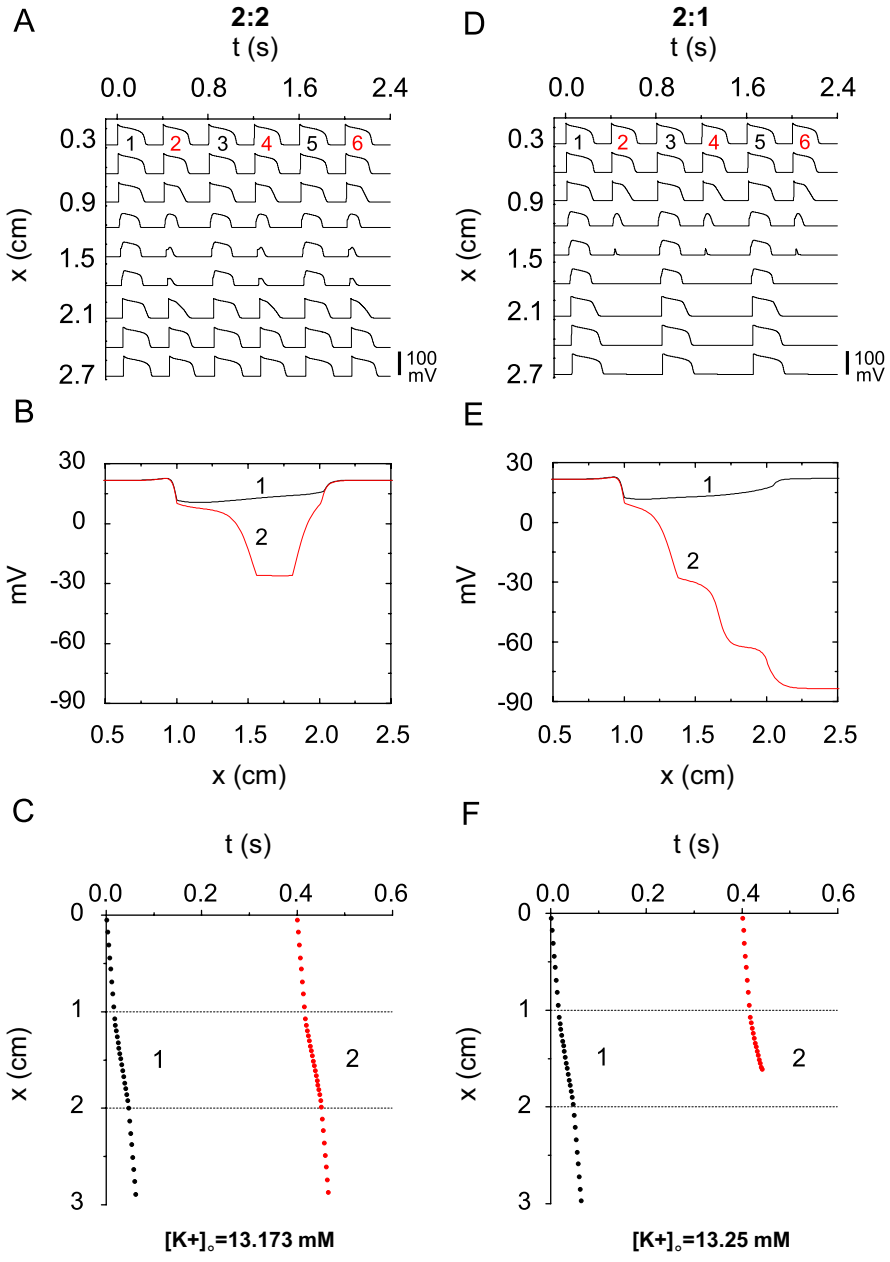

Fig. 2. *Period-2 rhythms*: Left column (A–C): 2:2 rhythm, $[K^+]_o = 13.173$ mM; right column (D–F): 2:1 rhythm, $[K^+]_o = 13.25$ mM. Same format as Fig. 1, except that in (B) and (E), V_{max} is plotted for more than one beat and *RMP* is not plotted.

potential, there is also a beat-to-beat alternation in the conduction time through the ischemic segment, which is just barely discernible in the laddergram of Fig. 2C. The smaller APD and conduction velocity of the even-numbered beats are both presumably accounted for by the fact that the diastolic interval or recovery time preceding them is less than that preceding the odd-numbered beats (Fig. 2A).

With further increase in $[K^+]_o$ to just beyond ~13.219 mM, the maintained small-amplitude response of the 2:2 rhythm (even-numbered beats in Fig. 2A–C) is replaced by a decrementing response (even-numbered beats in Fig. 2D–F: $[K^+]_o = 13.25$ mM) that eventually blocks within the distal half of the ischemic segment. The 2:2 rhythm is thus converted into a 2:1 rhythm, with the recovery time preceding the conducted beat being longer than that preceding the blocked beat, the more so with increasing penetration into the ischemic segment (Fig. 2D).

3.3. Higher-order rhythms

Still further increase in $[K^+]_o$ eventually results in the 2:1 rhythm converting into a 4:2 rhythm (Fig. 3A–C: $[K^+]_o = 13.437$ mM). A full-sized action potential (*beat 1*),

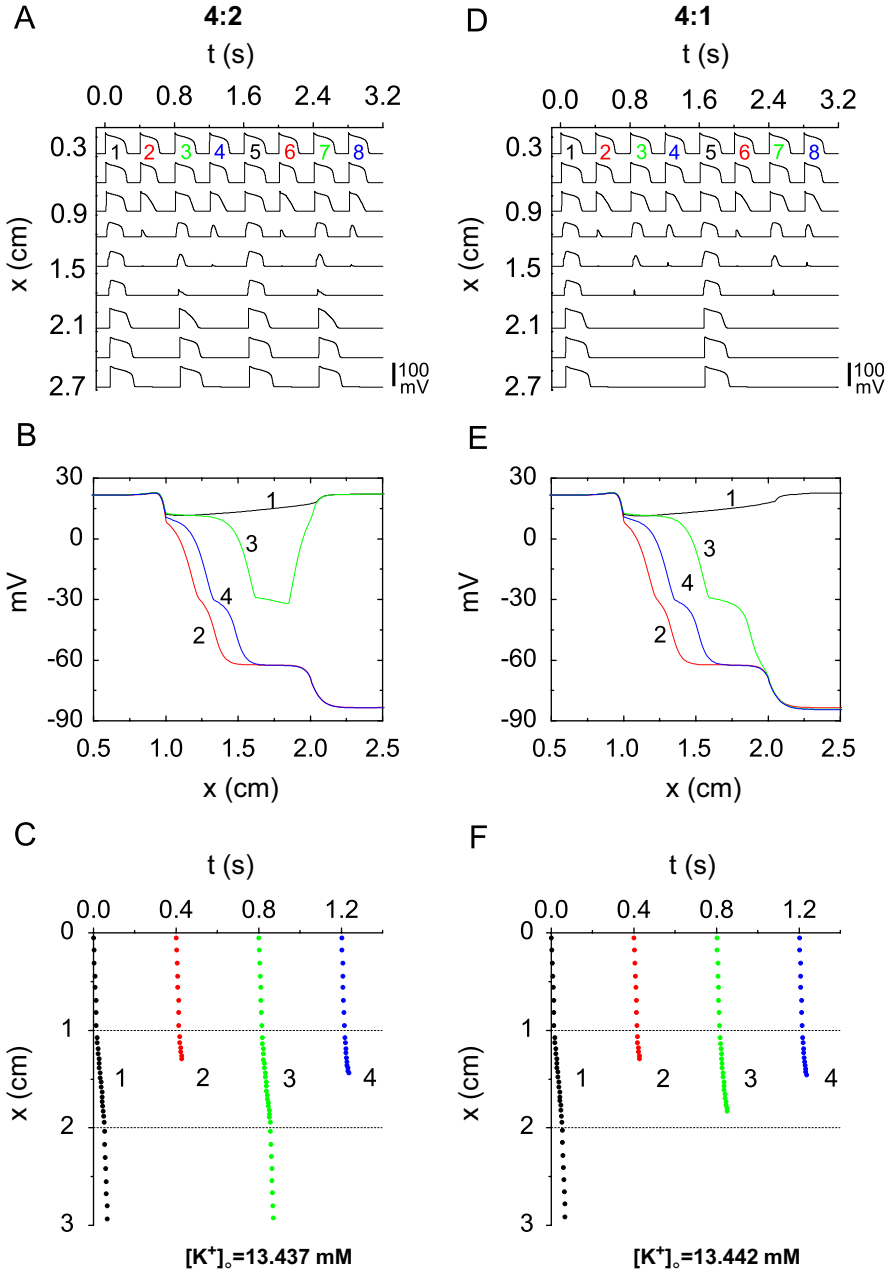

Fig. 3. *Period-4 rhythms*: Left column (A–C): 4:2 rhythm, $[K^+]_o = 13.437$ mM; right column (D–F): 4:1 rhythm, $[K^+]_o = 13.442$ mM. Same format as Fig. 2.

which is the first conducted beat in Fig. 3A, is followed by a blocked beat (*beat 2*), which is in turn followed by a maintained small-amplitude response (*beat 3*) that is the second conducted beat of the cycle. This second conducted beat is then followed by the second blocked beat of the cycle (*beat 4*), whereupon the period-4 cycle repeats. Note that there is an alternation in the depth to which the ischemic segment is penetrated by the two blocked beats (Fig. 3C), with the blocked beat (*beat 4*) that follows the small-amplitude response (*beat 3*) penetrating more deeply than the blocked beat (*beat 2*) that follows the full-sized action potential (*beat 1*), presumably because the recovery time before *beat 4* is longer than that preceding *beat 2*. As $[K^+]_o$ is raised still further, *beat 3* of this 4:2 rhythm increasingly decrements, eventually blocking within the ischemic segment, yielding a 4:1 rhythm (Figs. 3D–F: $[K^+]_o = 13.442$ mM).

With still further increase in $[K^+]_o$, the above process is repeated, resulting first in a 6:2 rhythm (Fig. 4A–C: $[K^+]_o = 13.472$ mM). The fifth beat in this rhythm (the maintained small-amplitude response) eventually dies out with further increase in $[K^+]_o$ (Fig. 4D–F: $[K^+]_o = 13.476$ mM), producing a 6:1 rhythm in the same way that a 4:1 rhythm arose out of a 4:2 rhythm in Fig. 3.

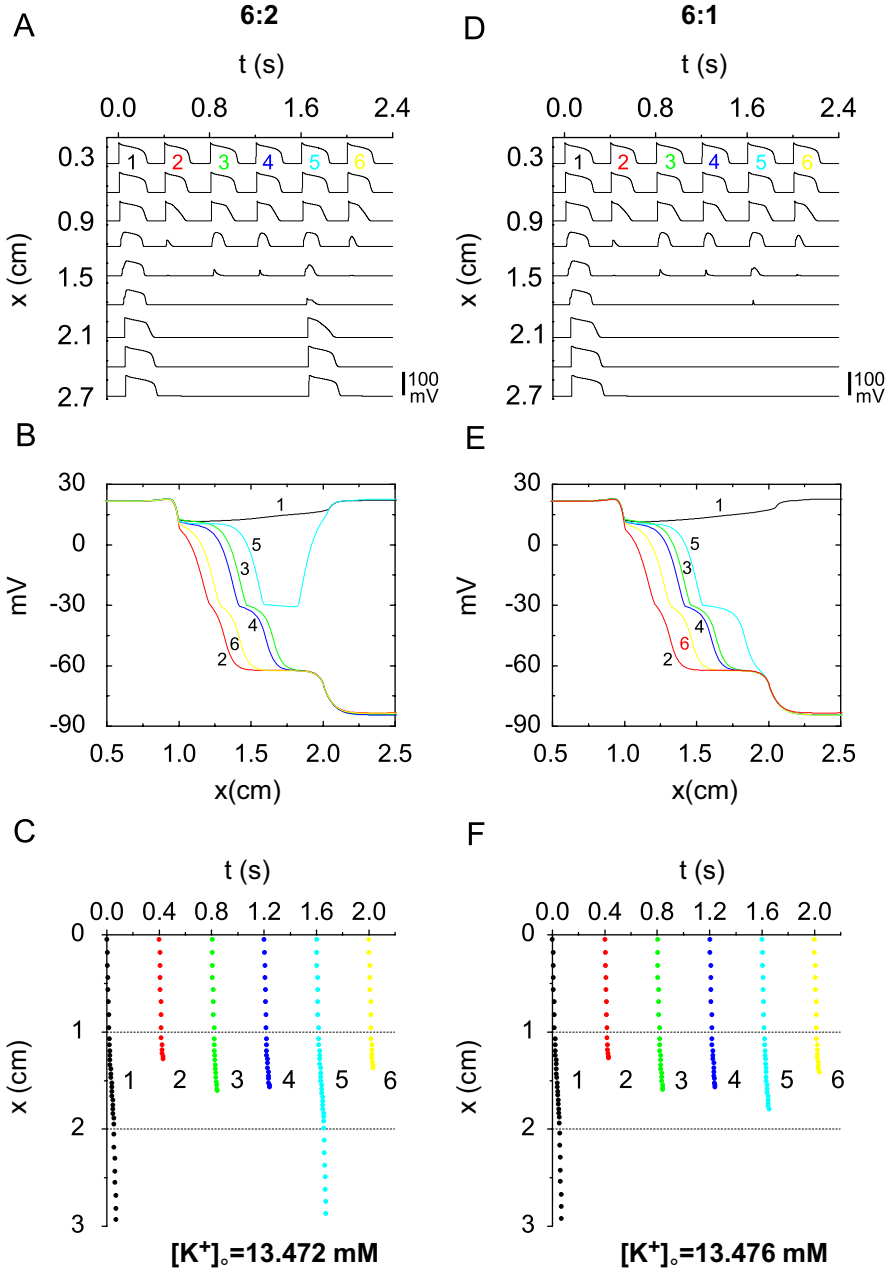

Fig. 4. *Period-6 rhythms*: Left column (A–C): 6:2 rhythm, $[K^+]_o = 13.472$ mM; right column (D–F): 6:1 rhythm, $[K^+]_o = 13.476$ mM. Same format as Fig. 2.

As $[K^+]_o$ is raised further, there are then 8:2 (Fig. 5A–C: $[K^+]_o = 13.4855$ mM) and 8:1 (Fig. 5D–F: $[K^+]_o = 13.487$ mM) rhythms.

Each cycle of the 6:2 rhythm consists of alternating 4:1 and 2:1 cycles (Fig. 4C), and not two different 3:1 cycles, as, e.g., one would expect if the 6:2 rhythm arose out of a period-doubling of a 3:1 rhythm. In the same way, an 8:2 cycle is made up of alternating 6:1 and 2:1 cycles (Fig. 5C), and not two different 4:1 cycles, as one would expect from a period-doubling of a 4:1 rhythm. This is in contrast to the 2:2 rhythm, each cycle of which is composed of two different 1:1 cycles (Fig. 2A), and the 4:2 rhythm, each cycle of which contains two different 2:1 cycles (Fig. 3A). In these higher-order (i.e., $N>2$) N:M rhythms, there is a beat-to-beat alternation in the depth of penetration of the ischemic segment by the blocked beats.

3.4. Subthreshold rhythms

Beyond the 8:1 rhythm, one encounters n:0 rhythms of complete block, in which no action potentials survive to the distal end of the cable, so that the rhythm sufficiently distal in the cable is entirely subthreshold. A 2:0 rhythm is first seen, with both action potentials of the cycle dying out within the ischemic segment (Fig. 6A–C: $[K^+]_o = 13.494$ mM). There is again a beat-to-beat alternation

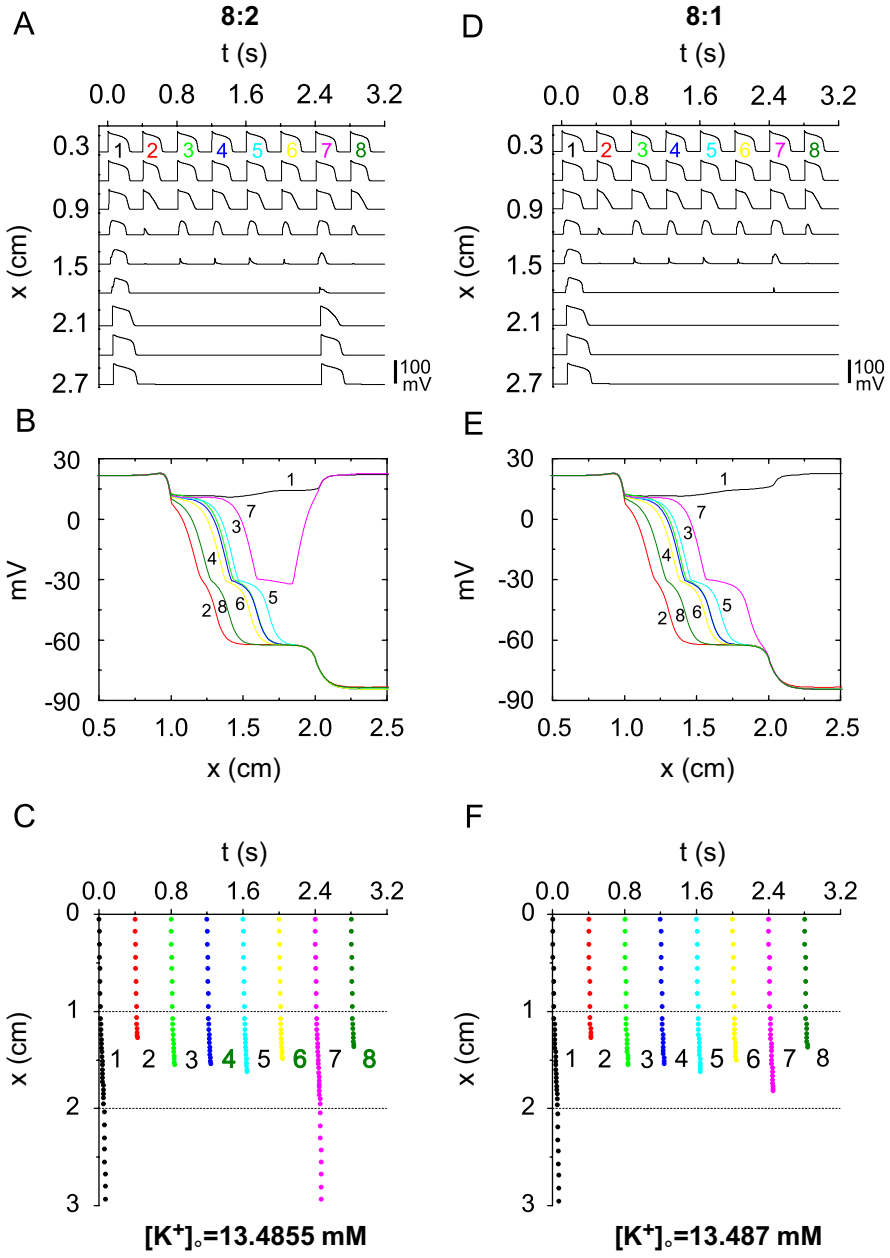

Fig. 5. *Period-8 rhythms*: Left column (A–C): 8:2 rhythm, $[K^+]_o = 13.4855$ mM; right column (D–F): 8:1 rhythm, $[K^+]_o = 13.487$ mM. Same format as Fig. 2.

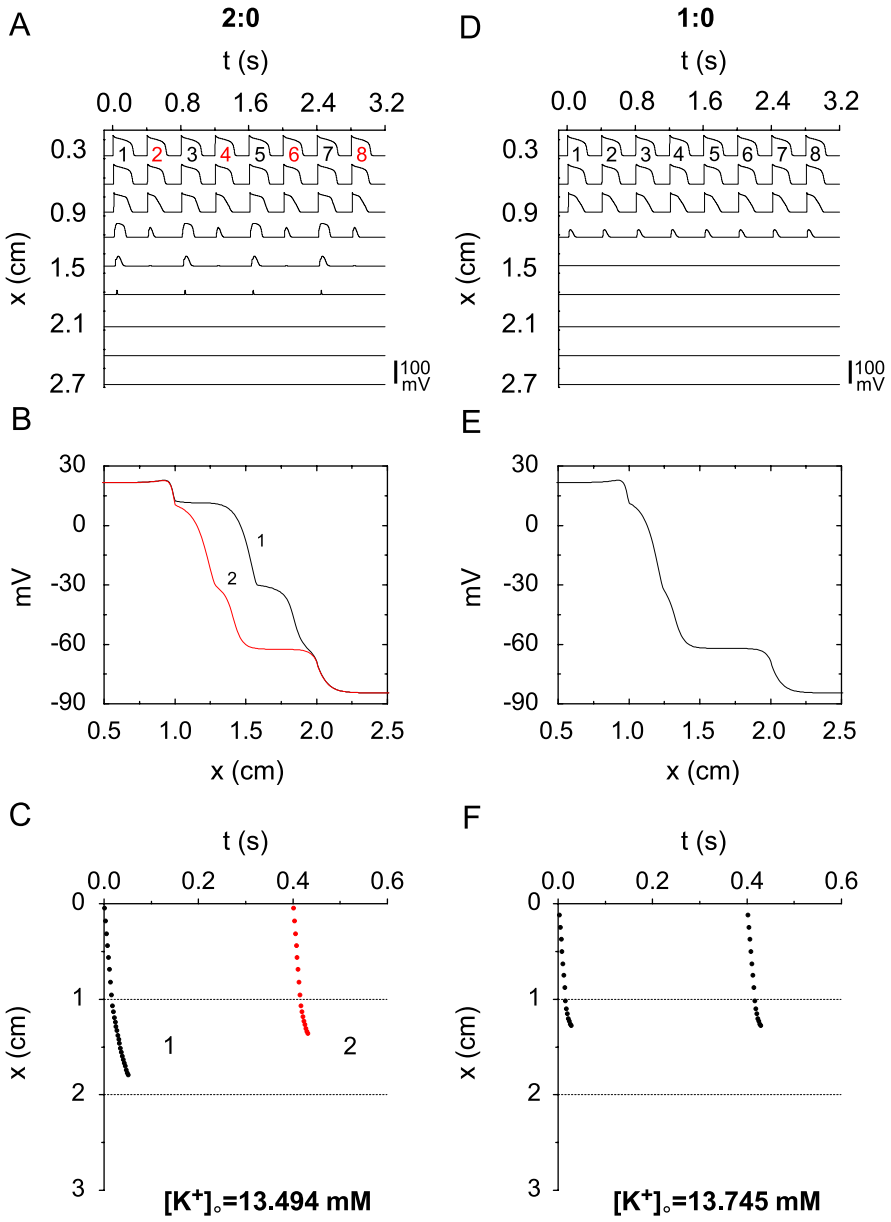

Fig. 6. *Subthreshold rhythms*: Left column (A–C): 2:0 rhythm, $[K^+]_o = 13.494$ mM; right column (D–F): 1:0 rhythm, $[K^+]_o = 13.745$ mM. Same format as Fig. 2.

in the depth of penetration into the ischemic segment (Fig. 6C), with the odd-numbered beats, which are preceded by the longer recovery time (Fig. 6A), penetrating more deeply than the even-numbered beats. For sufficiently high $[K^+]_o$, one finds the 1:0 rhythm of classic complete block (Fig. 6D–F: $[K^+]_o = 13.745$ mM) (Cranefield et al., 1971). At the $[K^+]_o$ in Fig. 6E, all action potentials start to block immediately upon entering the ischemic segment.

3.5. Bifurcation diagram

Fig. 7 is a bifurcation diagram, summarizing the results described above. Our bifurcation index is the normalized voltage integral (*NVI*), obtained by adding together the voltages at all elements in the cable on each fifth integration time-step, adding these summed values over the entire 400 ms stimulation period, and then normalizing by dividing this sum by the corresponding value obtained at the nominal $[K^+]_o$ of 5.4 mM (Arce et al., 2002). In this one-parameter bifurcation diagram, the bifurcation index *NVI* is plotted vs. the bifurcation parameter $[K^+]_o$.

Fig. 7A illustrates that rhythms other than 1:1 and 1:0 (open red symbols) are found over only an exceedingly narrow range of $[K^+]_o$. Fig. 7B shows the {1:1→2:2→2:1} transition: an *NVI* of ~0.6 during 2:2 rhythm corresponds to the maintained small-amplitude response (Figs. 2A–C), while an *NVI* of ~0.4 during 2:1 rhythm corresponds to the blocked beat (Figs. 2D–F). The {2:1→4:2→4:1}, {4:1→6:2→6:1}, {6:1→8:2→8:1}, and {8:1→2:0→1:0} transitions are illustrated in Fig. 7C–F, respectively.

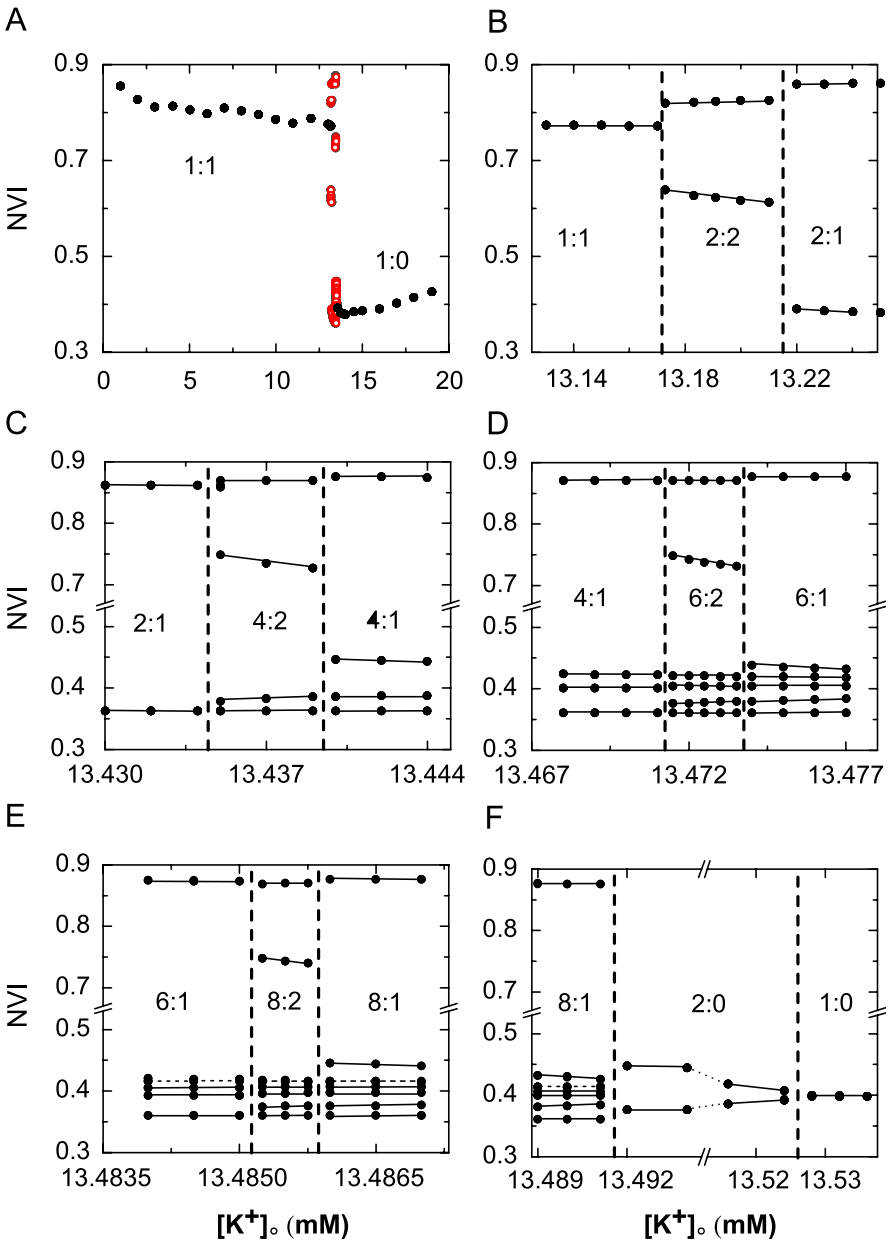

Fig. 7. *Bifurcation diagram*: The normalized voltage integral (*NVI*) is plotted as a function of $[K^+]_o$: (A) overall bifurcation diagram. Closed black circles indicate period-1 rhythms; open red circles indicate non-period-1 rhythms; (B) {1:1→2:2→2:1} transitions; (C) {2:1→4:2→4:1} transitions; (D) {4:1→6:2→6:1} transitions; (E) {6:1→8:2→8:1} transitions; and (F) {8:1→2:0→1:0} transitions. The dashed line in (E) and (F) indicates two lines that superimpose on the scale of this diagram. To avoid excessive crowding of symbols, not all points computed are plotted. The computed $[K^+]_o$ ranges are (mM): 1.0–13.170 (1:1); 13.171–13.219 (2:2); 13.220–13.434 (2:1); 13.436–13.439 (4:2); 13.440–13.471 (4:1); 13.4715–13.473 (6:2); 13.474–13.485 (6:1); 13.48525–13.48575 (8:2); 13.486–13.4911 (8:1); 13.4912–13.524 (2:0); 13.528–19.0 (1:0).

3.6. Other lengths of the ischemic segment

During ongoing ischemia, not only does $[K^+]_o$ gradually increase, but the physical size of the ischemic zone gradually grows. We have thus carried out additional simulations in which $[K^+]_o$ is increased in a cable with a central ischemic segment that has a length (L) different from the nominal value of 1 cm used above, maintaining the lengths of both adjacent normal segments at 1 cm. The two-parameter ($[K^+]_o$, L) bifurcation diagram of Fig. 8 summarizes our results. We have not explored all values of L in this diagram with increments in $[K^+]_o$ as fine as those used in constructing Fig. 7 ($L = 1$ cm). Nevertheless, one can already see that the sequence of rhythms encountered as $[K^+]_o$ is increased is not the same at all L.

As L is reduced below 1 cm (e.g., $L = 0.5$ cm), elevation of $[K^+]_o$ eventually results in a 3:1 rhythm (very small area at lower-right in Fig. 8), which we do not encounter at $L = 1$ cm. Fig. 9 shows examples of the 2:1 ($[K^+]_o = 13.571$ mM) and 3:1 ($[K^+]_o = 13.574$ mM) rhythms encountered at $L = 0.5$ cm. During the 2:1 rhythm, the blocked beat is preceded by a much shorter recovery time

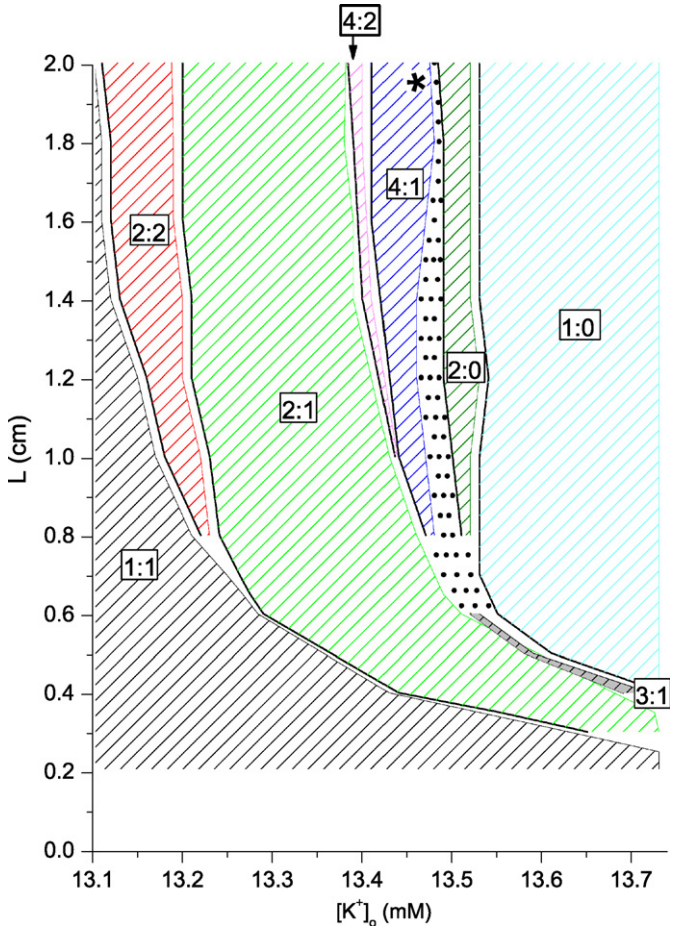

Fig. 8. *Global bifurcation diagram*: Rhythm seen at a particular combination of external potassium concentration ($[K^+]_o$) and length of the ischemic segment (L). Exploration is first made on a coarse grid (step-size for $[K^+]_o$ is 0.05 mM; step-size for L is 0.2 cm, starting at $L = 0.2$ cm). Finer steps are then used to explore the boundaries between different zones. Other rhythms (e.g. 6:2, 6:1, 8:2, 8:1, 5:2, 4:0) are found in the stippled area. The asterisk at the top of the 4:1 zone indicates a very small 8:2 zone.

than the conducted beat (Fig. 9A), as it is in the $L = 1$ cm cable (Fig. 2D). During the 3:1 rhythm the blocked beat that penetrates the ischemic segment more deeply (*beat 3*) is preceded by a recovery time that is considerably longer than that preceding the other blocked beat (*beat 2*), which does not penetrate as deeply. But while the recovery time preceding the conducted beat (*beat 1*, or equivalently *beat 4*) is longer than that preceding the first blocked beat (*beat 2*), it is shorter than that preceding the second blocked beat (*beat 3*), demonstrating that the simple concept of recovery time is not enough to explain the dynamics here. (A similar consideration applies when one examines the two conducted beats of the 4:2 rhythm in Fig. 3A, where, in the more proximal elements of the cable, the full-sized action potential (*beat 1*) is preceded by a recovery time that is slightly shorter than that preceding the maintained small-amplitude response (*beat 3*).) The transition from 2:1 to 3:1 rhythm at $L = 0.5$ cm is not direct, since, e.g., a 5:2 rhythm can be found at an intermediate value of $[K^+]_o$ (13.572 mM).

While it cannot be appreciated on the scale of Fig. 8, for L sufficiently larger than 1 cm (e.g., $L = 2.0$ cm), the 6:2 and 6:1 rhythms encountered at $L = 1$ cm (Fig. 4) are no longer seen, and there is instead a direct transition from a 4:1 rhythm (similar to that shown in Fig. 3) at $[K^+]_o = 13.4558$ mM to an 8:2 rhythm at $[K^+]_o = 13.4560$ mM (asterisk at the top of the 4:1 zone in Fig. 8). This 8:2 rhythm consists of two different 4:1 cycles that alternate, with the conducted beat being a full-sized action potential in one 4:1 cycle, and a maintained subthreshold response in the other 4:1 cycle. This 8:2 rhythm is thus very different from the 8:2 rhythm seen at $L = 1$ cm (Fig. 5A–C), in which there is an alternation between 2:1 and 6:1 cycles. Should the transition here from 4:1 to 8:2 rhythm be a supercritical period-doubling bifurcation, the transition would be direct, with no intervening rhythms (e.g., period-6) being necessary (it is impossible to rule out the presence of period-6 rhythms using numerical integration runs; however, in the absence of bistability, any such rhythms would have to exist over a range of $[K^+]_o$ of less than 0.0002 mM). At $L = 2.0$ cm, further increase in $[K^+]_o$ leads to a reversion from the 8:2 rhythm back to a 4:1 rhythm in which the conducted action potential is a maintained subthreshold response. (See Supplementary Material III for movies of these two different 4:1 rhythms and the 8:2 rhythm.) At the highest values of $[K^+]_o$ at $L = 2$ cm, one sees 4:0, 2:0, and 1:0 rhythms. More careful exploration of Fig. 8 is needed to work out definitively the bifurcation sequences, which have been explored very minutely only for $L = 1$ cm (Fig. 7).

4. Discussion

4.1. Period-2 rhythms in the ischemic ventricle

Alternans is commonly seen during acute myocardial ischemia and often presages the imminent onset of malignant phase-1A reentrant ventricular arrhythmias in experimental work (see references in Introduction; see Narayan (2006) for clinical applications). Our simulations reveal two mechanisms underlying alternans. In the first scenario, there is a 2:2 rhythm within a circumscribed region, with a 2:1 rhythm being present nowhere else (Fig. 2A–C): "primary" alternans (Guevara, 1988). Unfortunately, in experimental work one cannot prove the existence of primary alternans, given that it is impossible with present-day recording techniques to rule out the presence of some small—perhaps only intramural—area of 2:1 block. In the second scenario (Fig. 2D), there are coexisting areas of 2:2 and 2:1 rhythm, as is found in the ischemic ventricle (Downar et al., 1977; Hashimoto et al., 1984; Carson et al., 1986; Abe et al., 1989). This "secondary" alternans (Fig. 2D–F) has also been seen in a false tendon with a central segment exposed to high $[K^+]_o$ (Cranefield et al., 1971), as well as in modelling of an inhomogeneous

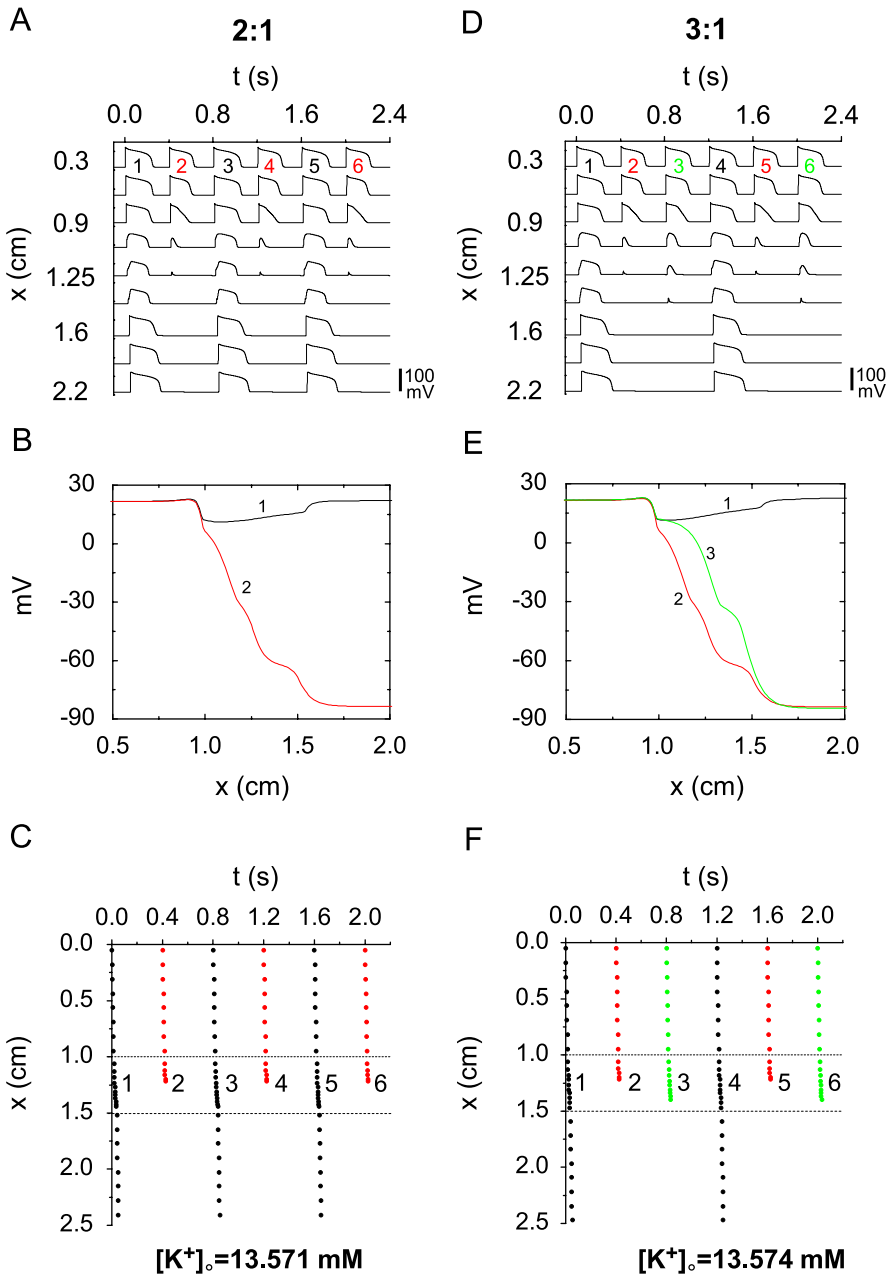

Fig. 9. *Period-3 rhythm*: Length of ischemic segment: 0.5 cm. Left column (A–C): 2:1 rhythm, $[K^+]_o = 13.571$ mM; right column (D–F): 3:1 rhythm, $[K^+]_o = 13.574$ mM. Same format as Fig. 2, but traces in (A) and (D) taken at $x = 0.3$, 0.6, 0.9, 1.1, 1.25, 1.4, 1.6, 1.9 and 2.2 cm.

Purkinje fibre cable (Guevara, 1988). In our simulations (Fig. 7B and C), primary alternans occurs over a much narrower range of $[K^+]_o$ than secondary alternans (see Section 1 of Supplementary Material II for further discussion of this point).

One often sees a gradual increase in the magnitude of alternans ("crescendo alternans," Dilly and Lab, 1988) in the extracellular recording (Downar et al., 1977; Russell et al., 1979; Abe et al., 1989; Nearing et al., 1991; Nearing and Verrier, 2002) that often heralds the onset of ventricular fibrillation (see, e.g., Fig. 3A(C) in Nearing and Verrier, 2002). This increase is likely due to a progressive extension in the size of the areas of 2:2 rhythm and 2:1 block, with a progressive conversion of areas initially showing 2:2 rhythm into areas showing 2:1 block (Fig. 3 of Downar et al., 1977; Fig. 1 of Russell et al., 1979; Fig. 12 of Hashimoto et al., 1984).

4.2. *Higher-order rhythms arise out of alternans and presage tachyarrhythmias*

As ischemia progresses, the simultaneous gradual rise in $[K^+]_o$ and gradual expansion of the ischemic area (Coronel et al., 1988) would correspond to movement along a path upwards and to the right in Fig. 8. Our computations thus predict that immediately after alternans occurs, but

before complete block develops, higher-order rhythms (e.g., period-3, -4, -6, -8) would be seen.

While there have been scattered incidental reports of period-3 rhythms (Russell et al., 1979; Hashimoto et al., 1984) and period-4 rhythms (Dilly and Lab, 1988; Laguna et al., 1999; Wu and Zipes, 2001) during acute ischemia, there has been thus far only one systematic experimental search for period-3 and period-4 rhythms (Nearing and Verrier, 2002). Six of the 12 dogs in that study fibrillated during the 8-min coronary occlusion period. In five of these six dogs, alternans was followed by either a period-3 or a period-4 rhythm, then by "complex" non-repeating rhythms, and then by fibrillation; the remaining animal showed only very high-amplitude alternans before fibrillation occurred (Figs. 2 and 3 of Nearing and Verrier, 2002). Of the six other animals that did not fibrillate, four showed only alternans (two of which were at a very low level), and the remaining two stayed in period-1 rhythm.

The narrowness of the range of $[K^+]_o$ over which higher-order rhythms exist (Figs. 7 and 8) leads us to predict that stable higher-order rhythms would be exceedingly difficult to observe during rapidly evolving myocardial ischemia. Estimating a rate of increase of $[K^+]_o$ on the order of $\sim 1\,mM\,min^{-1}$ in the central zone (this rate is highly variable, is considerably less in the border zone, and declines with time (Figs. 1 and 4B of Hill and Gettes, 1980; Fig. 2(b) of Coronel et al., 1988), one can calculate from our results that one would expect to see period-4 rhythms, which exist over a $[K^+]_o$ range of at most $\sim 0.1\,mM$ (Fig. 8), for only a few seconds. In the experimental work, period-3 and period-4 rhythms, which occurred during the last minute or so before fibrillation started up, lasted on average for 26 and 23 s, and were "inherently unstable and evanescent"; indeed, the existence of a higher-order periodic rhythm was established on the basis of as few as two consecutive cycles (Nearing and Verrier, 2002).

In the presence of temporal noise and spatial inhomogeneity, one expects "bifurcation gaps," in which periodic rhythms existing in the noise-free state over only very narrow ranges, as well as rhythms of sufficiently long period, are replaced by non-periodic rhythms (Crutchfield and Huberman, 1980). In Fig. 8, for $L > \sim 0.8\,cm$, one might thus observe, in the presence of a bifurcation gap, only the sequence {period-1 → 2 → 4 → complete block}, or perhaps even only {period-1 → 2 → complete block}; for $\sim 0.4\,cm < L < \sim 0.6\,cm$, one might expect to see {period-1 → 2 → 3 → complete block}, or perhaps even only {period-1 → 2 → complete block}. Indeed, the sequence {1:1 → 2:2 → 2:1 → 1:0} has been reported during ischemia (Downar et al., 1977). In instances where only a period-2 rhythm has been reported before the onset of fibrillation (Downar et al., 1977; Russell et al., 1979; Cinca et al., 1980; Hashimoto et al., 1984; Carson et al., 1986; Dilly and Lab, 1988; Abe et al., 1989; Konta et al., 1990; Tachibana et al., 1998), it is possible that occult higher-order rhythms would have been identified had more sensitive signal-detection techniques (Martínez and Olmos, 2005) been used.

Should the rate of increase of $[K^+]_o$ be sufficiently great, one would traverse the region of higher-order rhythms in Fig. 8 in a time shorter than that necessary to see a single cycle of a higher-order rhythm. Indeed, in the one dog that fibrillated with a direct transition from alternans to ventricular fibrillation, there was a very much faster rate of increase of alternans amplitude than in the remaining five dogs that showed higher-order rhythms before fibrillating (Fig. 3A(C) of Nearing and Verrier, 2002). There also are 1-D maps that can display a transition to chaos following a finite number—as small as one or two—of apparent bifurcations (Tresser et al., 1980; Mayer-Kress and Haken, 1984; Chialvo et al., 1990; Nusse and Yorke, 1992; Watanabe et al., 1995).

4.3. Is complete block necessary for reentry?

Since 2:1 block can proceed on to complete block within the core of the ischemic zone (Downar et al., 1977; Coronel et al., 1988), one can argue that complete block is obligatory at some location in order to provide the inexcitable obstacle that would allow classic circus-movement reentry. Indeed, one can estimate from Fig. 8 that the time-lag between the onset of a period-4 rhythm and the onset of complete block would be on the order of only a few seconds, which is consistent with the time-lag observed in the experiments between the onset of the period-4 rhythms and the onset of complex rhythms (Nearing and Verrier, 2002). Since the electrogram gives the electrical activity averaged over some portion of the ventricular muscle, when alternans or a higher-order rhythm is identified in the electrogram, there might be one or more zones of complete block present, given the great heterogeneity of the ischemic ventricle. Since detailed activation mapping of the onset of the arrhythmias that follow higher-order rhythms during ischemia has not yet been reported, one does not know whether complete block occurs within the ischemic zone some time following the onset of higher-order rhythms, but just before fibrillation starts and, if so, whether this might be the crucial initiating event.

4.4. Origin of period-2 and period-4 rhythms during ischemia

In 3/5 dogs demonstrating higher-order rhythms and fibrillation, the sequence seen was {period-1 → 2 → 4 → complex → fibrillation} (Nearing and Verrier, 2002). It was then suggested that this corresponds to the classic period-doubling route, in which there is a cascade of an infinite number of period-doubling bifurcations leading to deterministically aperiodic ("chaotic") dynamics (May, 1976). This route to chaos exists in paced cardiac tissue (Guevara et al., 1981; Hescheler and Speicher, 1989; Savino et al., 1989; Chialvo et al., 1990; Gilmour et al., 1997). In the presence of bifurcation gaps, the {1:1 → 2:2 → 2:1 → 4:2 → 4:1 → … → 1:0} sequence of Fig. 7 might be converted

into the sequence {period-1→2→4→complete block}—rhythms of period higher than 4 were not searched for in Nearing and Verrier (2002). The voltage traces in Figs. 2 and 3 are suggestive of period-doubling bifurcations in the {1:1→2:2} and {2:1→4:2} transitions. We have been unable to establish this, with the ticklish numerical results leading to an effectively discontinuous 1-D map in the former case (Arce et al., 2002). The {2:2→2:1} and {4:2→4:1} transitions are reminiscent of changes in firing number (Othmer and Xie, 1999).

The sequence {1:1→2:2→2:1→4:2→chaos} has been described in paced tissue (Chialvo et al., 1990) and in ionic models (Lewis and Guevara, 1990; Vinet et al., 1990). While it is possible that period-8 and even higher-order period-doubled rhythms were not found due to a bifurcation gap, discontinuous 1-D maps can display chaotic dynamics following as few as two period-doubling bifurcations (Lewis and Guevara, 1990).

Yet another explanation for the {period-1→2→4→…} sequence would be a {1:1→2:1} transition (Yehia et al., 1999), followed by a {2:1→4:1} transition. Coexisting areas of period-2 and period-4 rhythms (Nearing and Verrier, 2002) as well as 2:1 and 4:1 block (but not 3:1 block) (Wu and Zipes, 2001) have been reported during ischemia.

For further discussion about chaos, see Section 4 of Supplementary Material II.

4.5. Origin of period-3 rhythms during ischemia

In 2/6 dogs, the sequence seen was {period-1→2→3→complex→fibrillation} (Nearing and Verrier, 2002). The fact that these period-3 rhythms occurred later (by ~23 s) than the period-4 rhythms seen in three other dogs was taken as being consistent with the classic period-doubling route, where the period-3 orbit occurs later that the period-doubled and period-quadrupled orbits (May, 1976). But in both cases of period-3 rhythm, the preceding period-2 rhythm lasted for quite a long time, and so one might have expected to have seen other higher-order periodic and chaotic rhythms for a rather long time after the period-2 rhythm ceased, but before the period-3 rhythm appeared (see, e.g., Fig. 4 of May, 1976). Instead, the period-3 rhythm arose directly out of a long-lasting period-2 rhythm (Nearing and Verrier, 2002).

A second scenario here is an effectively direct {2:1→3:1} or {2:2→3:2} transition. The 2:1 and 3:1 zones lie very close to one another in Fig. 8, so that in the presence of a bifurcation gap one would have a {2:1→3:1} transition. This transition to a period-3 rhythm takes place at a higher level of $[K^+]_o$ than does the transition to period-4 rhythm, which might account for the later appearance of the former rhythm in the experiments. Ischemic alternans can be accompanied by "varying degrees of conduction blocks with either 2:1, 3:1, or more irregular patterns of endocardial–epicardial conduction block" (Russell et al., 1979), and there can be the co-existence of period-2 and period-3 rhythms at different locations (Hashimoto et al., 1984).

A third scenario here is the sequence {1:1→2:2→2:1→4:2→chaos→3:1→6:2→…}. In one case, the ranges of the period-doubled (2:2, 4:2, 6:2) and chaotic rhythms were so narrow that, in the presence of even a very small bifurcation gap, one would expect to see the reduced sequence {period-1→2→3} (see Fig. 5(a) of Lewis and Guevara, 1990).

A fourth scenario occurs in piecewise-smooth systems, where a period-2 orbit can make a direct transition to a period-3 orbit via a border-collision bifurcation (Nusse and Yorke, 1992).

For further discussion about the bifurcations underlying period-2 and higher-order rhythms, see Section 3 of Supplementary Material II.

4.6. Subthreshold rhythms

The 1:0 rhythm of Fig. 6D–F (classic complete block) has been reported in the ischemic ventricle (Downar et al., 1977; Cinca et al., 1980; Coronel et al., 1988, 1989). The fall in action potential amplitude with distance (Fig. 6E) occurs in false tendons in which the middle segment is exposed to high $[K^+]_o$ (Cranefield et al., 1971). The subthreshold 2:0 rhythm (Fig. 6A–C) has been described in the ischemic ventricle (Cinca et al., 1980), in the space-clamped squid giant axon (Kaplan et al., 1996), the space-clamped FitzHugh–Nagumo equations (Rajasekar and Lakshmanan, 1988; Kaplan et al., 1996), and in homogeneous 1-D FitzHugh–Nagumo (Horikawa, 1994) and Hodgkin–Huxley (Horikawa, 1998) cables of reduced excitability.

The transition from 1:0 to 2:0 rhythm (Fig. 6) appears to be due to a period-doubling bifurcation. While there can be a cascade of these period-doubling bifurcations that culminates in subthreshold chaotic dynamics (Rajasekar and Lakshmanan, 1988; Horikawa, 1994, 1998; Kaplan et al., 1996), we have not encountered this in our simulations at $L = 1$ cm, changing $[K^+]_o$ in steps of 0.0001 mM. We see three possible explanations for this absence. First, higher-order period-doubled subthreshold rhythms and subthreshold chaotic rhythms might exist over an exquisitely narrow range of $[K^+]_o$. Second, higher-order periodic and aperiodic subthreshold rhythms simply might not exist: the forward period-doubling cascade might be incomplete and be terminated by a partial reverse cascade of period-halving bifurcations (Horikawa, 1998). Third, if bistability is present, these rhythms would not have been encountered if our computations did not start out from within their basins of attraction.

4.7. Atrioventricular block

Our model of regional ischemia can also be taken as a crude model of the atrioventricular node, with the proximal normal segment representing the right atrium, the ischemic segment representing the atrioventricular

(AV) node, and the distal normal segment representing the His bundle. There are many correspondences of our results with experimental and clinical findings during AV block. It is known that 3:1 AV block is rare: "In experiment, 4:1 block is much more frequent than 3:1 block" (Lewis, 1920) (cf. our Fig. 8). In Figs. 2–5, 2*N*:2 rhythms are seen, in which there is an alternation of the conduction time, in the absence of longitudinal dissociation ("dual pathways") (Pick et al., 1962; Watanabe and Dreifus, 1972). Direct transitions between 2:1 and 4:1, 4:1 and 6:1, and 6:1 and 8:1 AV block have been documented (Castellanos et al., 1998; see also Fig. 252 of Lewis, 1920). In paced strips of fetal sheep epicardial muscle, a sequence of period-4, -6, and -8 rhythms uncannily similar to those seen in our cable was described (Watanabe et al., 1995). Direct transitions between 4:1 and 8:1 AV block can occur (Castellanos et al., 2005). There are multiple levels of concealment of blocked responses (Watanabe and Dreifus, 1972), as in Figs. 3–5. Finally, in the proximal elements of the cable in Fig. 3A, there is behavior reminiscent of supernormal AV conduction (Pick et al., 1962).

4.8. Limitations of the model

The ventricles are 3-D and we use a 1-D structure, so that effects due to, e.g., anisotropy and transmural fibre axis rotation, cannot occur. Large-scale gradients (e.g., apex-to-base and endocardial-to-epicardial gradients in APD), as well as inhomogeneities on a smaller scale, are not included. While we represent the effects of ischemia by changing $[K^+]_o$, it is well-known that other factors, such as hypoxia, acidosis, and Ca^{2+}-cycling play a considerable role. We have set a sharp demarcation between the normal zone and the ischemic zone, but there is in fact a graded border zone. Our model is a guinea-pig model, and since most experiments on ischemia have been done in larger animals (typically dogs and pigs), species differences may play a confounding role.

4.9. Future work

Recording of the transmembrane potential from many sites, e.g., with the optical-dye technique (Wu and Zipes, 2001; Lakireddy et al., 2005) will help in elucidating the nature of any causal relationship between higher-order rhythms and the induction of reentrant rhythms and also in discriminating amongst the various rhythms that can all give rise to a period-*n* rhythm on the electrogram (e.g., 3:2 Wenckebach and 3:1 block both result in a period-3 rhythm). Further modelling work should remove some of the limitations of the present model mentioned immediately above. In particular, since Ca^{2+}-cycling can theoretically generate higher-order rhythms (Qu et al., 2007), it will be interesting to see how any such rhythms intrinsically generated in an ionic model of space-clamped membrane might interact with the rhythms of higher-order block described above. However, it might take some time to work out the teething problems in the rather complicated second-generation models that allow Ca^{2+}-cycling (see, e.g., Cherry and Fenton, 2007). The modelling work should be expanded to consider the later stages of ischemia (e.g., phase 1b), when cellular uncoupling occurs (Pollard et al., 2002). The close temporal association of discordant alternans, higher-order rhythms, and spiral-wave reentry (Nearing and Verrier, 2002; Bernus et al., 2005) cries out for further investigation (see also Section 2 of Supplementary Material II). The 1-D map analysis accounting for the $\{1{:}1 \to 2{:}2 \to 2{:}1\}$ sequence (Arce et al., 2002) should be extended to higher-order transitions. Finally, will it be possible to make connections between higher-order rhythms, discordant alternans, and the induction of reentry—presumably spiral-wave in origin—using a low-dimensional analysis?

Acknowledgements

Supported by grants to HA from PAPIIT-UNAM (Grant no. IN109307), and to MRG from the Canadian Institutes of Health Research (MOP-43846). We thank Enrique Palacios Boneta for help in programming and Dr. Max Lab for pointing out to us the existence of a period-4 rhythm in one of his papers. This work forms the M.Sc. thesis of one of the authors (AL).

Appendix. Supplementary materials

The online version of this article contains three sets of additional material: a listing of the modified Luo–Rudy model (Supplementary Material I), some additional discussion (Supplementary Material II), and movies corresponding to Figs. 1–6 and 9, as well as three other movies (Supplementary Material III). Please visit doi:10.1016/j.jtbi.2007.06.015.

References

Abe, S., Nagamoto, Y., Fukuchi, Y., Hayakawa, T., Kuroiwa, A., 1989. Relationship of alternans of monophasic action potential and conduction delay inside the ischemic border zone to serious ventricular arrhythmia during acute myocardial ischemia in dogs. Am. Heart J. 117, 1223–1233.

Arce, H., Xu, A., González, H., Guevara, M.R., 2000. Alternans and higher-order rhythms in an ionic model of a sheet of ischemic ventricular muscle. Chaos 10, 411–426.

Arce, H., López, A., Guevara, M.R., 2002. Triggered alternans in an ionic model of ischemic cardiac ventricular muscle. Chaos 12, 807–818.

Beeler, G.W., Reuter, H., 1977. Reconstruction of the action potential of ventricular myocardial fibres. J. Physiol. (London) 268, 177–210.

Bernus, O., Wilders, R., Zemlin, C.W., Verschelde, H., Panfilov, A.V., 2002. A computationally efficient electrophysiological model of human ventricular cells. Am. J. Physiol. Heart Circ. Physiol. 282, H2296–H2308.

Bernus, O., Zemlin, C.W., Zaritsky, R.M., Mironov, S.F., Pertsov, A.M., 2005. Alternating conduction in the ischaemic border zone as precursor of reentrant arrhythmias: a simulation study. Europace 7, S93–S104.

Carmeliet, E., 1999. Cardiac ionic currents and acute ischemia: from channels to arrhythmias. Physiol. Rev. 79, 917–1017.

Carson, D.L., Cardinal, R., Savard, P., Vermeulen, M., 1986. Characterisation of unipolar waveform alternation in acutely ischaemic porcine myocardium. Cardiovasc. Res. 20, 521–527.

Castellanos, A., Moleiro, F., Pastor, J.A., Interian Jr., A., Myerburg, R.J., 1998. Reverse alternating Wenckebach periods and other modes of regression of $\geqslant$8:1 to 2:1 atrioventricular block. Am. J. Cardiol. 82, 528–531.

Castellanos, A., Diaz, J., Interian Jr., A., Myerburg, R.J., 2005. Wenckebach's periods or alternating Wenckebach's periods during 4:1 atrioventricular block? J. Electrocardiol. 38, 157–159.

Cherry, E.M., Fenton, F.H., 2007. A tale of two dogs: analyzing two models of canine ventricular electrophysiology. Am. J. Physiol. Heart Circ. Physiol. 292, H43–H55.

Chialvo, D.R., Gilmour Jr., R.F., Jalife, J., 1990. Low dimensional chaos in cardiac tissue. Nature 343, 653–657.

Cimponeriu, A., Starmer, C.F., Bezerianos, A., 1998. Action potential propagation in ischemic cardiac tissue: a theoretical computer modeling. Computers in Cardiology 1998. IEEE Computer Society, New York, NY, pp. 317–320.

Cinca, J., Janse, M.J., Moréna, H., Candell, J., Valle, V., Durrer, D., 1980. Mechanism and time course of the early electrical changes during acute coronary artery occlusion. Chest 77, 499–505.

Coronel, R., Fiolet, J.W.T., Wilms-Schopman, F.J.G., Schaapherder, A.F.M., Johnson, T.A., Gettes, L.S., Janse, M.J., 1988. Distribution of extracellular potassium and its relation to electrophysiologic changes during acute myocardial ischemia in the isolated perfused porcine heart. Circulation 77, 1125–1138.

Coronel, R., Fiolet, J.W.T., Wilms-Schopman, F.J.G., Opthof, T., Schaapherder, A.F.M., Janse, M.J., 1989. Distribution of extracellular potassium and electrophysiologic changes during two-stage coronary ligation in the isolated, perfused canine heart. Circulation 80, 165–177.

Cranefield, P.F., Klein, H.O., Hoffman, B.F., 1971. Conduction of the cardiac impulse. I. Delay, block, and one-way block in depressed Purkinje fibers. Circ. Res. 28, 199–219.

Crutchfield, J.P., Huberman, B.A., 1980. Fluctuations and the onset of chaos. Phys. Lett. A 77, 407–410.

Dilly, S.G., Lab, M.J., 1988. Electrophysiological alternans and restitution during acute regional ischaemia in myocardium of anaesthetized pig. J. Physiol. (London) 402, 315–333.

Downar, E., Janse, M.J., Durrer, D., 1977. The effect of acute coronary artery occlusion on subepicardial transmembrane potentials in the intact porcine heart. Circulation 56, 217–224.

Feldman, A.B., Esperer, H.D., Cohen, R.J., 1999. A mechanism controlling the characteristics of T-wave alternans measurements in the setting of myocardial ischemia. Computers in Cardiology 1999. IEEE Computer Society, Piscataway, NJ, pp. 149–152.

Ferrero Jr., J.M., Torres, V., Saiz, J., Monserrat, M., Ferrero, J.M., Thakor, N.V., 1997. Simulation study of action potentials during acute myocardial ischemia. Computers in Cardiology 1997. IEEE Computer Society, New York, NY, pp. 705–708.

Ferrero Jr., J.M., Trénor, B., Rodríguez, B., Sáiz, J., 2003. Electrical activity and reentry during acute regional myocardial ischemia: insights from simulations. Int. J. Bifurc. Chaos 13, 3703–3715.

Gilmour Jr., R.F., Otani, N.F., Watanabe, M.A., 1997. Memory and complex dynamics in cardiac Purkinje fibers. Am. J. Physiol. Heart Circ. Physiol. 272, H1826–H1832.

Guevara, M.R., 1988. Spatiotemporal patterns of block in an ionic model of cardiac Purkinje fibre. In: Markus, M., Müller, S.C., Nicolis, G. (Eds.), From Chemical to Biological Organization. Springer, Berlin, pp. 273–281.

Guevara, M.R., Glass, L., Shrier, A., 1981. Phase locking, period-doubling bifurcations, and irregular dynamics in periodically stimulated cardiac cells. Science 214, 1350–1353.

Hashimoto, H., Asano, M., Nakashima, M., 1984. Potentiating effects of a ventricular premature beat on the alternation of the ST-T complex of epicardial electrograms and the incidence of ventricular arrhythmias during acute coronary occlusion in dogs. J. Electrocardiol. 17, 289–301.

Hescheler, J., Speicher, R., 1989. Regular and chaotic behaviour of cardiac cells stimulated at frequencies between 2 and 20 Hz. Eur. Biophys. J. 17, 273–280.

Hill, J.L., Gettes, L.S., 1980. Effect of acute coronary artery occlusion on local myocardial extracellular K^+ activity in swine. Circulation 61, 768–778.

Horikawa, Y., 1994. Period-doubling bifurcations and chaos in the decremental propagation of a spike train in excitable media. Phys. Rev. E 50, 1708–1710.

Horikawa, Y., 1998. Bifurcations in the decremental propagation of a spike train in the Hodgkin–Huxley model of low excitability. Biol. Cybern. 79, 251–261.

Isenberg, G., Klöckner, U., 1982. Calcium currents of isolated bovine ventricular myocytes are fast and of large amplitude. Pflüg. Arch.-Eur. J. Physiol. 395, 30–41.

Janse, M.J., van Capelle, F.J.L., Morsink, H., Kléber, A.G., Wilms-Schopman, F., Cardinal, R., Naumann D'Alnoncourt, C., Durrer, D., 1980. Flow of "injury" current and patterns of excitation during early ventricular arrhythmias in acute regional myocardial ischemia in isolated porcine and canine hearts. Evidence for two different arrhythmogenic mechanisms. Circ. Res. 47, 151–165.

Kaplan, D.T., Clay, J.R., Manning, T., Glass, L., Guevara, M.R., Shrier, A., 1996. Subthreshold dynamics in periodically stimulated squid giant axons. Phys. Rev. Lett. 76, 4074–4077.

Koller, M.L., Riccio, M.L., Gilmour Jr., R.F., 2000. Effects of $[K^+]_o$ on electrical restitution and activation dynamics during ventricular fibrillation. Am. J. Physiol. Heart Circ. Physiol. 279, H2665–H2672.

Konta, T., Ikeda, K., Yamaki, M., Nakamura, K., Honma, K., Kubota, I., Yasui, S., 1990. Significance of discordant ST alternans in ventricular fibrillation. Circulation 82, 2185–2189.

Krogh-Madsen, T., Schaffer, P., Skriver, A.D., Taylor, L.K., Pelzmann, B., Koidl, B., Guevara, M.R., 2005. An ionic model for rhythmic activity in small clusters of embryonic chick ventricular cells. Am. J. Physiol. Heart Circ. Physiol. 289, H398–H413.

Laguna, P., Moody, G.B., Garcia, J., Goldberger, A.L., Mark, R.G., 1999. Analysis of the ST-T complex of the electrocardiogram using the Karhunen–Loève transform: adaptive monitoring and alternans detection. Med. Biol. Eng. Comput. 37, 175–189.

Lakireddy, V., Baweja, P., Syed, A., Bub, G., Boutjdir, M., El-Sherif, N., 2005. Contrasting effects of ischemia on the kinetics of membrane voltage and intracellular calcium transient underlie electrical alternans. Am. J. Physiol. Heart Circ. Physiol. 288, H400–H407.

Lewis, T., 1920. The Mechanism and Graphic Registration of the Heart Beat. Shaw & Sons, London.

Lewis, T.J., Guevara, M.R., 1990. Chaotic dynamics in an ionic model of the propagated cardiac action potential. J. Theor. Biol. 146, 407–432.

Linz, K.W., Meyer, R., 2000. Profile and kinetics of L-type calcium current during the cardiac ventricular action potential compared in guinea-pigs, rats and rabbits. Pflüg. Arch.-Eur. J. Physiol. 439, 588–599.

Luo, C.-H., Rudy, Y., 1991. A model of the ventricular cardiac action potential. Depolarization, repolarization, and their interaction. Circ. Res. 68, 1501–1526.

Martínez, J.P., Olmos, S., 2005. Methodological principles of T wave alternans analysis: a unified framework. IEEE Trans. Biomed. Eng. 52, 599–613.

May, R.M., 1976. Simple mathematical models with very complicated dynamics. Nature 261, 459–467.

Mayer-Kress, G., Haken, H., 1984. Attractors of convex maps with positive Schwarzian derivative in the presence of noise. Physica D 10, 329–339.

Narayan, S.M., 2006. T-wave alternans and the susceptibility to ventricular arrhythmias. J. Am. Coll. Cardiol. 47, 269–281.

Nearing, B.D., Verrier, R.L., 2002. Progressive increases in complexity of T-wave oscillations herald ischemia-induced ventricular fibrillation. Circ. Res. 91, 727–732.

Nearing, B.D., Verrier, R.L., 2003. Tracking cardiac electrical instability by computing interlead heterogeneity of T-wave morphology. J. Appl. Physiol. 95, 2265–2272.

Nearing, B.D., Huang, A.H., Verrier, R.L., 1991. Dynamic tracking of cardiac vulnerability by complex demodulation of the T wave. Science 252, 437–440.

Nusse, H.E., Yorke, J.A., 1992. Border-collision bifurcations including "period two to period three" for piecewise smooth systems. Physica D 57, 39–57.

Othmer, H.G., Xie, M., 1999. Subharmonic resonance and chaos in forced excitable systems. J. Math. Biol. 39, 139–171.

Pick, A., Langendorf, R., Katz, L.N., 1962. The supernormal phase of atrioventricular conduction. I. Fundamental mechanisms. Circulation 26, 388–404.

Pollard, A.E., Cascio, W.E., Fast, V.G., Knisley, S.B., 2002. Modulation of triggered activity by uncoupling in the ischemic border: a model study with phase 1b-like conditions. Cardiovasc. Res. 56, 381–392.

Qu, Z., Shiferaw, Y., Weiss, J.N., 2007. Nonlinear dynamics of cardiac excitation–contraction coupling: an iterated map study. Phys. Rev. E 75, 011927.

Rajasekar, S., Lakshmanan, M., 1988. Period doubling route to chaos for a BVP oscillator with periodic external force. J. Theor. Biol. 133, 473–477.

Russell, D.C., Smith, H.J., Oliver, M.F., 1979. Transmembrane potential changes and ventricular fibrillation during repetitive myocardial ischaemia in the dog. Br. Heart J. 42, 88–96.

Savino, G.V., Romanelli, L., González, D.L., Piro, O., Valentinuzzi, M.E., 1989. Evidence for chaotic behavior in driven ventricles. Biophys. J. 56, 273–280.

Scherlag, B.J., El-Sherif, N., Hope, R., Lazzara, R., 1974. Characterization and localization of ventricular arrhythmias resulting from myocardial ischemia and infarction. Circ. Res. 35, 372–383.

Sharp, G.H., Joyner, R.W., 1980. Simulated propagation of cardiac action potentials. Biophys. J. 31, 403–423.

Shaw, R.M., Rudy, Y., 1997. Electrophysiologic effects of acute myocardial ischemia. A mechanistic investigation of action potential conduction and conduction failure. Circ. Res. 80, 124–138.

Tachibana, H., Kubota, I., Yamaki, M., Watanabe, T., Tomoike, H., 1998. Discordant S-T alternans contributes to formation of reentry: a possible mechanism of reperfusion arrhythmia. Am. J. Physiol. Heart Circ. Physiol. 275, H116–H121.

ten Tusscher, K.H.W.J., Panfilov, A.V., 2003. Reentry in heterogeneous cardiac tissue described by the Luo–Rudy ventricular action potential model. Am. J. Physiol. Heart Circ. Physiol. 284, H542–H548.

Tilg, B., Wach, P., 1995. Simulation of the 1-D cardiac excitation process by varying extracellular potassium concentration and intracellular resistivity. Computers in Cardiology 1995. IEEE Computer Society, New York, NY, pp. 421–424.

Tresser, C., Coullet, P., Arneodo, A., 1980. On the existence of hysteresis in a transition to chaos after a single bifurcation. J. Phys. Lett. (Paris) 41, L243–L246.

Vinet, A., Chialvo, D.R., Michaels, D.C., Jalife, J., 1990. Nonlinear dynamics of rate-dependent activation in models of single cardiac cells. Circ. Res. 67, 1510–1524.

Wang, Y., Rudy, Y., 2000. Action potential propagation in inhomogeneous cardiac tissue: safety factor considerations and ionic mechanism. Am. J. Physiol. Heart Circ. Physiol. 278, H1019–H1029.

Watanabe, Y., Dreifus, L.S., 1972. Levels of concealment in second degree and advanced second degree A-V block. Am. Heart J. 84, 330–347.

Watanabe, M., Otani, N.F., Gilmour Jr., R.F., 1995. Biphasic restitution of action potential duration and complex dynamics in ventricular myocardium. Circ. Res. 76, 915–921.

Wit, A.L., Janse, M.J., 1993. The Ventricular Arrhythmias of Ischemia and Infarction. Electrophysiological Mechanisms. Futura, Mount Kisco.

Wu, J., Zipes, D.P., 2001. Transmural reentry during acute global ischemia and reperfusion in canine ventricular muscle. Am. J. Physiol. Heart Circ. Physiol. 280, H2717–H2725.

Xu, A., Guevara, M.R., 1998. Two forms of spiral-wave reentry in an ionic model of ischemic ventricular myocardium. Chaos 8, 157–174.

Yehia, A.R., Jeandupeux, D., Alonso, F., Guevara, M.R., 1999. Hysteresis and bistability in the direct transition from 1:1 to 2:1 rhythm in periodically driven single ventricular cells. Chaos 9, 916–931.

SUPPLEMENTARY MATERIAL I ("IONIC MODEL EQUATIONS")

A. López *et al.*:
"Rhythms of high-grade block in an ionic model of a strand of regionally ischemic ventricular muscle"

***Membrane potential* (V)**

$$dV/dt = -(I_{\mathrm{Na}} + I_{si} + I_{\mathrm{K}} + I_{\mathrm{K1}} + I_{\mathrm{Kp}} + I_b)/C_m, \quad \text{with } C_m = 1\ \mu\mathrm{F/cm}^2.$$

Ionic concentrations

$$[\mathrm{Na}]_{\mathrm{o}} = 140\ \mathrm{mM}, \qquad [\mathrm{Ca}]_{\mathrm{o}} = 1.8\ \mathrm{mM}, \qquad [\mathrm{Na}]_{\mathrm{i}} = 18\ \mathrm{mM}, \qquad [\mathrm{K}]_{\mathrm{i}} = 145\ \mathrm{mM}.$$

Reversal potentials

$$E_{\mathrm{Na}} = (RT/F)\log_e([\mathrm{Na}]_{\mathrm{o}}/[\mathrm{Na}]_{\mathrm{i}}).$$
$$E_{\mathrm{K1}} = E_{\mathrm{Kp}} = (RT/F)\log_e([\mathrm{K}]_{\mathrm{o}}/[\mathrm{K}]_{\mathrm{i}}).$$
$$E_{\mathrm{K}} = (RT/F)\log_e[([\mathrm{K}]_{\mathrm{o}} + PR_{\mathrm{NaK}}[\mathrm{Na}]_{\mathrm{o}})/([\mathrm{K}]_{\mathrm{i}} + PR_{\mathrm{NaK}}[\mathrm{Na}]_{\mathrm{i}})], \quad PR_{\mathrm{NaK}} = 0.01833.$$

***Fast inward Na^+ current* (I_{Na})**

$$I_{\mathrm{Na}} = 23m^3hj(V - E_{\mathrm{Na}}).$$
$$dm/dt = \alpha_{\mathrm{m}}(1-m) - \beta_{\mathrm{m}}m, \qquad dh/dt = \alpha_{\mathrm{h}}(1-h) - \beta_h h, \qquad dj/dt = \alpha_{\mathrm{j}}(1-j) - \beta_{\mathrm{j}}j.$$

For $V \geq -40$ mV:

$$\alpha_h = 0.$$
$$\beta_h = 1/(0.13\{1 + \exp[-(V + 10.66)/11.1]\}).$$
$$\alpha_j = 0.$$
$$\beta_j = 0.3\exp(-2.535\times10^{-7}V)/\{1 + \exp[-0.1(V+32)]\}.$$

For $V < -40$ mV:

$$\alpha_h = 0.135\exp[-(80+V)/6.8].$$
$$\beta_{\mathrm{h}} = 3.56\exp(0.079\mathrm{V}) + 3.1\times10^5\exp(0.35\mathrm{V}).$$
$$\alpha_j = [-1.2714\times10^5\exp(0.2444V) - 3.474\times10^{-5}\exp(-0.04391V)](V+37.78)/$$
$$\{1 + \exp[0.311(V+79.23)]\}.$$
$$\beta_j = 0.1212\exp(-0.01052V)/\{1 + \exp[-0.1378(V+40.14)]\}.$$

For all V:

$\alpha_m = 0.32(V + 47.13)/\{1 - \exp[-0.1(V + 47.13)]\}.$

$\beta_m = 0.08\exp(-V/11).$

***Slow inward Ca^{++} current* (I_{si})**

$I_{si} = 0.09df(V - E_{si}), \quad E_{si} = 7.7 - 13.0287\log_e([\mathrm{Ca}]_\mathrm{i}).$

$dd/dt = \alpha_\mathrm{d}(1-d) - \beta_\mathrm{d} m, \qquad df/dt = \alpha_\mathrm{f}(1-f) - \beta_f f.$

$\alpha_d = 0.95\exp[-0.01(V-5)]/\{1 + \exp[-0.072(V-5)]\}.$

$\beta_d = 0.7\exp[-0.017(V+44)]/\{1 + \exp[0.05(V+44)]\}.$

$\alpha_f = 0.012\exp[-0.008(V+28)]/\{1 + \exp[0.15(V+28)]\}.$

$\beta_f = 0.0065\exp[-0.02(V+30)]/\{1 + \exp[-0.2(V+30)]\}.$

$d([Ca]_\mathrm{i})/dt = -10^{-4} I_{si} + 0.07(10^{-4} - [Ca]_\mathrm{i}).$

***Delayed rectifier K^+ current* (I_K)**

$I_\mathrm{K} = \bar{G}_\mathrm{K} x X_i (V - E_\mathrm{K}), \qquad \bar{G}_K = 0.282\sqrt{[\mathrm{K}]_\mathrm{o}/5.4}.$

$dx/dt = \alpha_\mathrm{x}(1-x) - \beta_\mathrm{x} x.$

$\alpha_x = 0.0005\exp[0.083(V+50)]/\{1 + \exp[0.057(V+50)]\}.$

$\beta_x = 0.0013\exp[-0.06(V+20)]/\{1 + \exp[-0.04(V+20)]\}.$

$X_i = 2.837\{\exp[0.04(V+77)] - 1\}/\{(V+77)\exp[0.04(V+35)]\}.$

***Inward rectifier K^+ current* (I_{K1})**

$I_{\mathrm{K1}} = \bar{G}_{\mathrm{K1}} K1_\infty (V - E_{\mathrm{K1}}), \qquad \bar{G}_{\mathrm{K1}} = 0.6047\sqrt{[\mathrm{K}]_\mathrm{o}/5.4}, \qquad \mathrm{K1}_\infty = \alpha_{\mathrm{K1}}/(\alpha_{\mathrm{K1}} + \beta_{\mathrm{K1}}).$

$\alpha_{K1} = 1.02/\{1 + \exp[0.2385(V - E_{K1} - 59.215)]\}.$

$\beta_{\mathrm{K1}} = \{0.49124 \bullet \exp[0.08032(V - E_{\mathrm{K1}} + 5.476)] + \exp[0.06175(V - E_{\mathrm{K1}} - 594.31)]\}/\{1 + \exp[-0.5143(V - E_{\mathrm{Kl}} + 4.753)]\}.$

***Plateau K^+ current* (I_{Kp})**

$$I_{\mathrm{Kp}} = 0.0183\mathrm{Kp}(V - E_{\mathrm{Kp}}).$$
$$\mathrm{Kp} = 1/\{1 + \exp[(7.488 - V)/5.98]\}.$$

***Background current* (I_b)**

$$I_b = 0.03921(V + 59.87).$$

In the above equations, voltage is in mV, time in ms, currents in μA/cm^2, rate constants in ms^{-1}, and ionic concentrations in mM. The value of *RT/F* is not mentioned in Luo and Rudy, 1991; we set *RT/F* = 26.7 mV. We set the values of α_d and β_d above to be 10 times larger than in the original Luo-Rudy model, so as to decrease the time constant τ_d for the activation of I_{si} ($\tau_d = 1/(\alpha_d + \beta_d)$) by a factor of 10, in order to bring τ_d into the physiologic range. L'Hôpital's rule is applied when an indeterminate form arises in the formulae for α_m and X_i. The alternative formula for X_i that applies for $V < -100$ mV (Luo and Rudy, 1991) is not needed here, since in our simulations $V > -100$ mV at all times. Programs in several different programming languages to numerically simulate the original Luo-Rudy model can be found on the world-wide web, e.g., http://cor.physiol.ox.ac.uk/ (for a recent listing of several other such repositories, see Table 4 in Wilders, 2007).

References

Luo, C.-H., Rudy, Y., 1991. A model of the ventricular cardiac action potential. Depolarization, repolarization, and their interaction. Circ. Res. 68:1501-1526.

Wilders, R., 2007. Computer modelling of the sinoatrial node. Med. Bio. Eng. Comput. 45:189–207.

SUPPLEMENTARY MATERIAL II ("ADDITIONAL DISCUSSION")

A. López *et al.*:
"Rhythms of high-grade block in an ionic model of a strand of regionally ischemic ventricular muscle"

1. Role of Raised $[K^+]_o$ in Inducing Period-2 Rhythms in the Ischemic Ventricle

We use a single intervention to model the electrophysiological effect of ischemia — a rise in $[K^+]_o$. Period-2 rhythms occur when $[K^+]_o$ is ~13 mM (Figs. 2,7B). In the pig ventricle, alternans has been detected 3–9 mins post-occlusion (Downar et al., 1977), during which time the average $[K^+]_o$ in the central ischemic zone is ~7–11 mM (Hill and Gettes, 1980; Coronel et al., 1988). However, the marked spatial heterogeneity in $[K^+]_o$ and in the electrophysiological response to ischemia (Downar et al., 1977; Hill and Gettes, 1980; Coronel et al., 1988; Coronel et al., 1989) would tend to result in alternans starting up at a time earlier than one might expect based on consideration of average $[K^+]_o$ alone: e.g., monophasic electrograms (indicating block within or into an area) are seen at 50% of electrode locations by the time that $[K^+]_o$ reaches 9-10 mM, and at over 90% of locations by 12 mM (Coronel et al., 1989). In addition, several other concurrent changes known to promote alternans and block (e.g., hypoxia, acidosis, internal Ca^{++}-cycling (Wit and Janse, 1993; Shaw and Rudy, 1997; Carmeliet, 1999; Ferrero Jr. et al., 2003; Bernus et al., 2005; Lakireddy et al., 2005; Carmeliet, 2006; Jordan and Christini, 2006; Qu et al., 2007) would undoubtedly lower the $[K^+]_o$ at which 2:2 and 2:1 rhythms would first be seen. Nevertheless, regional perfusion of the rabbit coronary system with a high-K^+ solution (≥ 9 mM) leads to both alternans and arrhythmias (Curtis, 1991) and similar experiments in the dog result in 2:1 endocardial-epicardial block and arrhythmias (Ettinger et al., 1973), indicating that elevated $[K^+]_o$ in and of itself can be a major cause of alternans, block, and tachyarrhythmias (see also modelling work of Bernus et al., 2005).

The fact that the 2:2 zone is so narrow in our simulations (~0.04 mM wide in Fig. 7B) implies that during ischemia the duration of the phase of primary alternans would be exceedingly brief — indeed almost certainly ephemeral —– before secondary alternans would ensue. At the time that alternans starts up, $[K^+]_o$ is rising at a rate on the order of 1 mM min^{-1} in the central ischemic zone (Hill and Gettes, 1980; Coronel et al., 1988), so that one would then predict from our simulations that the phase of primary alternans would last for a time on the order of only ~2.4 seconds (this estimate is very rough, given that the rate of increase of $[K^+]_o$ is highly variable from site to site, is considerably less in the border zone, and declines with time (Fig. 4B of Hill and Gettes, 1980; Fig. 2(b) of Coronel et al., 1988). In contrast, the 2:1 zone in Fig. 7B,C is much wider (~0.2 mM), so that the phase of secondary alternans would be predicted to last for ~12 seconds. This is considerably shorter than the mean duration of ~82 seconds observed experimentally for alternans in the dog (Nearing and Verrier, 2002). This discrepancy is again likely due to the fact that in our model we are neglecting several germane factors that promote alternans (e.g., spatial inhomogeneity, hypoxia, acidosis, Ca^{++}-cycling).

Alternans and arrhythmias are commonly seen upon reperfusion following a period of coronary occlusion. The rapid premonitory increase in alternans amplitude (Downar et al., 1977; Carson et al., 1986; Nearing et al., 1991; Tachibana et al., 1998) might be accounted for by the fact that areas coming out of complete block start to produce action potentials (Downar et al., 1977). The resulting increase in spatiotemporal asynchrony almost certainly produces the inhomogeneity necessary for starting up reentrant rhythms (Downar et al., 1977). Again, $[K^+]_o$ is almost certainly playing a key role, since the very rapid fall in $[K^+]_o$ (much faster than the rate of

increase following occlusion (Hill and Gettes, 1980; Coronel et al., 1988)) has a time-course that parallels the much more rapid increase in alternans and arrhythmias seen following reperfusion (Downar et al., 1977; Curtis, 1991; Nearing et al., 1991). Furthermore, arrhythmias are seen following washout in experiments on regional coronary hyperkalemia (Curtis, 1991).

2. Alternans Does Not Necessarily Proceed Directly on to Reentrant Arrhythmias

In our modelling work of a two-dimensional sheet of regionally ischemic ventricular muscle, as $[K^+]_o$ increases in the ischemic zone, primary alternans occurs first, followed by 2:1 block, i.e., secondary alternans (Arce et al., 2000). When this 2:1 block occurs, the breaking of the excitation wavefront on every other beat creates a pair of nascent spiral wave-tips that might be expected to initiate a figure-of-eight spiral-wave reentrant rhythm, along the lines described in a recent modelling study on the effect of premature stimulation on a two-dimensional sheet of regionally ischemic ventricular muscle (Ferrero Jr. et al., 2003). However, reentrant arrhythmias were not seen; rather the 2:1 block proceeded on to higher-order rhythms and eventually complete block as $[K^+]_o$ was raised further. This finding in the model agrees with the experimental results, in so far that alternans does not typically lead directly to reentry, but rather to higher-order rhythms — in only 1/6 animals did fibrillation arise immediately out of alternans, without an intervening higher-order rhythm being seen (Nearing and Verrier, 2002). The rate of increase of the amplitude of the alternans in that animal was very high (Fig 3A(C) of Nearing and Verrier, 2002), so that it is all too conceivable that the range of $[K^+]_o$ over which higher-order rhythms exist was traversed too quickly for such rhythms to be seen. However, we have no firm explanation at present for why we did not see spiral-wave reentrant rhythms in our simulations following the onset of higher-order rhythms (and even complete block). Nevertheless, both the experimental and modelling work indicate that it is not obligatory that reentry occur immediately following a period-2 rhythm; indeed, the experimental results demonstrate that higher-order rhythms typically must occur first.

3. Bifurcations Responsible for Producing Period-2 and Higher-Order Rhythms

Perhaps the commonest way in which a period-2 rhythm arises directly out of a period-1 rhythm is *via* a supercritical period-doubling bifurcation (Guevara et al., 1981; Guevara et al., 1984). But this is not the only way: e.g., there can be a subcritical period-doubling bifurcation (Vinet and Roberge, 1994), or a saddle-node bifurcation of periodic orbits resulting in the creation *ex nihilo* of two period-2 orbits, one stable (corresponding to 2:2 rhythm), the other unstable (Singer, 1978; Mayer-Kress and Haken, 1984; Vinet and Roberge, 1994). A border-collision bifurcation has been implicated in producing the period-2 orbit underlying the PR–alternans seen in a model of time-delayed atrial stimulation (Chen et al., 1998).

When the atrium is paced at a gradually increasing rate, one eventually encounters 2:1 atrioventricular block. But consideration of a 1-dimensional map indicates that there can be mathematically an infinite number of different Wenckebach rhythms interposed between the 1:1 rhythm of normal sinus rhythm and the 2:1 rhythm of atrioventricular block (Guevara, 1991), so that the 2:1 rhythm of block cannot be said, on the basis of this one particular finding alone, to be a period-doubled rhythm arising directly out of a period-doubling bifurcation. In periodically driven isolated quiescent rabbit ventricular cells, the transition from 1:1 to 2:1 rhythm can be direct (Yehia et al., 1999), *via* a 2:2 rhythm (Guevara et al., 1989), or *via* Wenckebach-like

rhythms (Yehia et al., 1997), depending on the stimulus amplitude (analogous results are seen in spontaneously beating re-aggregates of embryonic chick ventricular cells (Guevara et al., 1990)).

In a similar vein, not all period-4 rhythms necessarily arise from a period-doubling of a period-doubled rhythm: e.g., a unimodal one-dimensional map such as the prototypical quadratic map has a second period-4 orbit that arises *via* a tangent or saddle-node bifurcation, and not *via* a cascade of two period-doubling bifurcations (May, 1976). This orbit is visited in the sequence ABCD (where A < B < C < D are the points of the orbit), whereas the true period-quadrupled orbit in the quadratic map has the ordering ACBD. The orbits constructed from return-maps obtained from our 4:2 and 4:1 rhythms at L = 1 cm (Fig. 3) have the ordering ACBD. In contrast, a 4:1 rhythm in which there is a monotonically increasing growth in the amplitude of the blocked responses (e.g., Bandura, 1980) will have the ordering ABCD. In the 4:2 rhythm of Fig. 3A, the two action potentials are not consecutive, being separated by a subthreshold response. However, this is not the only type of 4:2 rhythm that can exist: e.g., there is a different 4:2 rhythm in which each cycle consists of two consecutive action potentials followed by two consecutive subthreshold responses (Fig. 4B of Watanabe and Dreifus, 1972).

Similarly, a period-3 rhythm does not necessarily have to correspond to the particular period-3 orbit seen on a unimodal map, which arises *via* a saddle-node bifurcation and has the ordering ABC: e.g., one analysis of the 3:2 Wenckebach rhythm of atrioventricular block results in a period-2 orbit that visits both branches of a discontinuous map, each branch of which is monotonically increasing (Guevara, 1991). To avoid premature ─ and hence potentially misleading ─ attribution of a bifurcation route to the origin of a particular rhythm, we use the more neutral term period-2 (or period-4) rhythm, rather than period-doubled (or period-quadrupled) rhythm, in referring to a rhythm that has not necessarily been proven to arise out of one period-doubling bifurcation (or two successive period-doubling bifurcations); we have also used the terminology period-3 rhythm rather than period-tripled rhythm (Ritzenberg et al., 1984; Nearing and Verrier, 2002; Nearing and Verrier, 2003).

4. Chaos?

The exact nature and origin of the "complex" rhythms that follow higher-order rhythms during ischemia is unclear (Nearing and Verrier, 2003). One possibility is that these are higher-order periodic rhythms corrupted by stochastic effects due to temporal noise (e.g., membrane noise) and spatial noise (e.g., small-scale inhomogeneities in the ventricle). Indeed, the latter mechanism almost certainly accounts for the fact that different, rapidly changing rhythms are seen in adjacent areas of the ischemic ventricle, especially just before arrhythmias start up (Downar et al., 1977). While electrotonic interactions would help to maintain spatiotemporal synchrony, this becomes more difficult as the order of the rhythm increases, since smaller changes then suffice to destroy the rhythm, thus producing a bifurcation gap. It is also clear that when spatial heterogeneity is larger there will be a greater effect of noise in breaking up the temporal correlations between activity at different sites. It is thus perhaps not surprising that rather disordered ("complex") electrograms are seen following higher-order rhythms and just before reentrant beats occur during ischemia (Nearing and Verrier, 2003). There is also a considerable clinical literature on the impact upon arrhythmogenesis of spatiotemporal lability of repolarization: "QT dispersion" (beat-to-beat variability within a single electrocardiographic lead) and "T-wave complexity" (variability across different leads).

An alternative possibility to a stochastic mechanism is that the complex rhythms are deterministically chaotic. This prospect is particularly intriguing, given that the complex

rhythms proceed directly on to fibrillation, which appears to be due to spiral-wave break-up, which itself might be a form of spatiotemporal chaos (Strain and Greenside, 1998). Perhaps the best evidence to date for causal links between a bifurcation sequence, chaos, and arrhythmogenesis is in the rapidly paced toad ventricle, where the sequence {1:1 $\rightarrow$ 2:2 $\rightarrow$ 4:4 $\rightarrow$ chaos $\rightarrow$ arrhythmia} has been observed (Savino et al., 1989). In these chaotic rhythms there is one action potential for each stimulus. We have not seen any chaotic rhythms in our simulations. Should such rhythms in fact exist, they would cover minuscule areas in Fig. 8, leading to the conclusion that their relevance to the real world of experiment and the clinic would be minimal.

Another point of view is that there is no direct relationship between any putative chaotic pre-fibrillatory rhythm and any later chaotic fibrillatory rhythm. Since fibrillation can be bistable with normal sinus rhythm (as shown by the ability to fibrillate or defibrillate at will with a brief electrical shock), it might be that the pre-fibrillatory rhythm ─ chaotic or not ─ is simply setting up the initial conditions (e.g., unidirectional block) that allow the initiation of the reentrant rhythm that eventually terminates in fibrillation, whether that fibrillation itself be chaotic or not.

The claim has been made, alluding to the much-misapplied theorem of Li and Yorke (1975) that the existence of a period-3 rhythm ("tripling") implies the existence of all periodicities, as well as "pseudorandom" (i.e., deterministically chaotic) rhythms (Nearing and Verrier, 2002; see also Ritzenberg et al., 1984). However, this is not necessarily the case; e.g., a 3:2 Wenckebach rhythm, which is a period-3 rhythm, can be generated by a discontinuous two-branched map that yields neither period-doubled orbits nor chaos (Guevara, 1991). Other kinds of rhythms can also produce period-3 behaviour: e.g., a period-5 reverse Wenckebach 5:3 rhythm of atrioventricular block produces a "tripling" in the ventricular response (Fig. 1b of Ritzenberg et al., 1984). Indeed, it is not even clear at the present time that a one-dimensional map ─ much less one satisfying the more restrictive conditions of the Li-Yorke theorem ─ can account for the experimental results during ischemia.

It is almost certain, given the heterogeneity of the response to ischemia, that different sequences of rhythms occur in different individuals, and that there will be no universally observed one-parameter bifurcation sequence, even in the first few minutes of ischemia (e.g., Wenckebach rhythms have been described during acute ischemia (El-Sherif et al., 1975) and are characteristically seen in the 3-7-day-old infarct (El-Sherif et al., 1977)). It is already clear from Fig. 8 alone that the sequence of rhythms seen as ischemia progresses will depend on exactly which path is taken through this two-parameter bifurcation diagram, with both L and $[K^+]_o$ increasing as ischemia progresses. One also has to admit that in many cases in experimental work it will not be possible to definitively determine a complete bifurcation sequence due to the rapidly evolving substrate inherent during acute ischemia.

References

Arce, H., Xu, A., González, H., Guevara, M.R., 2000. Alternans and higher-order rhythms in an ionic model of a sheet of ischemic ventricular muscle. Chaos 10:411-426.

Bandura, J. P., 1980. The role of electrotonus in slow potential development and conduction in canine Purkinje tissue. In: Zipes, D.P., Bailey, J.C., Elharrar, V. (Eds.), The Slow Inward Current and Cardiac Arrhythmias. Martinus Nijhoff, The Hague, pp. 327-355.

Bernus, O., Zemlin, C.W., Zaritsky, R.M., Mironov, S.F., Pertsov, A.M., 2005. Alternating conduction in the ischaemic border zone as precursor of reentrant arrhythmias: A simulation study. Europace 7:S93-S104.

Carmeliet, E., 1999. Cardiac ionic currents and acute ischemia: from channels to arrhythmias. Physiol. Rev. 79:917-1017.

Carmeliet, E., 2006. Electrical alternans: membrane-limited and subcellular components. J Cardiovasc. Electrophysiol. 17:94-96.

Carson, D.L., Cardinal, R., Savard, P., Vermeulen, M., 1986. Characterisation of unipolar waveform alternation in acutely ischaemic porcine myocardium. Cardiovasc. Res. 20:521-527.

Chen, D., Wang, H. O., Chin, W., 1998. Suppressing cardiac alternans: analysis and control of a border-collision bifurcation in a cardiac conduction model. Proc. 1998 IEEE Internat. Symp. Circ. Syst. (ISCAS '98) 3:635-638.

Coronel, R., Fiolet, J.W.T., Wilms-Schopman, F.J.G., Opthof, T., Schaapherder, A.F.M., Janse, M.J., 1989. Distribution of extracellular potassium and electrophysiologic changes during two-stage coronary ligation in the isolated, perfused canine heart. Circulation 80:165-177.

Coronel, R., Fiolet, J.W.T., Wilms-Schopman, F.J.G., Schaapherder, A.F.M., Johnson, T.A., Gettes, L.S., Janse, M.J., 1988. Distribution of extracellular potassium and its relation to electrophysiologic changes during acute myocardial ischemia in the isolated perfused porcine heart. Circulation 77:1125-1138.

Curtis, M.J., 1991. The rabbit dual coronary perfusion model: a new method for assessing the pathological relevance of individual products of the ischaemic milieu: role of potassium in arrhythmogenesis. Cardiovasc. Res. 25:1010-1022.

Downar, E., Janse, M.J., Durrer, D., 1977. The effect of acute coronary artery occlusion on subepicardial transmembrane potentials in the intact porcine heart. Circulation 56:217-224.

El-Sherif, N., Scherlag, B.J., Lazzara, R., 1975. Electrode catheter recordings during malignant ventricular arrhythmia following experimental acute myocardial ischemia. Evidence for re-entry due to conduction delay and block in ischemic myocardium. Circulation 51:1003-1014.

El-Sherif, N., Scherlag, B.J., Lazzara, R., Hope, R.R., 1977. Re-entrant ventricular arrhythmias in the late myocardial infarction period. 1. Conduction characteristics in the infarction zone. Circulation 55:686-702.

Ettinger, P.O., Regan, T.J., Oldewurtel, H.A., Khan, M.I., 1973. Ventricular conduction delay and arrhythmias during regional hyperkalemia in the dog. Electrical and myocardial ion alterations. Circ. Res. 33:521-531.

Ferrero Jr., J.M., Trénor, B., Rodríguez, B., Sáiz, J., 2003. Electrical activity and reentry during acute regional myocardial ischemia: insights from simulations. Int. J. Bifurc. Chaos 13:3703-3715.

Guevara, M. R., 1991. Iteration of the human atrioventricular (AV) nodal recovery curve predicts many rhythms of AV block. In: Glass, L., Hunter, P., McCulloch, A. (Eds.), Theory of Heart. Springer-Verlag, New York, pp. 313-358.

Guevara, M. R., Alonso, F., Jeandupeux, D., van Ginneken, A.C.G., 1989. Alternans in periodically stimulated isolated ventricular myocytes: Experiment and model. In: Goldbeter, A. (Ed.), Cell to Cell Signalling: From Experiments to Theoretical Models. Harcourt Brace Jovanovich, London, pp. 551-563.

Guevara, M.R., Glass, L., Shrier, A., 1981. Phase locking, period-doubling bifurcations, and irregular dynamics in periodically stimulated cardiac cells. Science 214:1350-1353.

Guevara, M. R., Shrier, A., Glass, L., 1990. Chaotic and complex cardiac rhythms. In: Zipes, D.P., Jalife, J. (Eds.), Cardiac Electrophysiology: From Cell to Bedside. First Edition. W.B. Saunders, Philadelphia, pp. 192-201.

Guevara, M.R., Ward, G., Shrier, A., Glass, L., 1984. Electrical alternans and period-doubling bifurcations. Comp. Cardiol. 1984, IEEE Computer Society, Silver Spring, MD, pp. 167-170.

Hill, J.L., Gettes, L.S., 1980. Effect of acute coronary artery occlusion on local myocardial extracellular K^+ activity in swine. Circulation 61:768-778.

Jordan, P.N., Christini, D.J., 2006. Action potential morphology influences intracellular calcium handling stability and the occurrence of alternans. Biophys. J. 90:672-680.

Lakireddy, V., Baweja, P., Syed, A., Bub, G., Boutjdir, M., El-Sherif, N., 2005. Contrasting effects of ischemia on the kinetics of membrane voltage and intracellular calcium transient underlie electrical alternans. Am. J. Physiol. Heart Circ. Physiol. 288:H400-H407.

Li, T.-Y., Yorke, J.A., 1975. Period three implies chaos. Am. Math. Month. 82:985-992.

May, R.M., 1976. Simple mathematical models with very complicated dynamics. Nature 261:459-467.

Mayer-Kress, G., Haken, H., 1984. Attractors of convex maps with positive Schwarzian derivative in the presence of noise. Physica D 10:329-339.

Nearing, B.D., Huang, A.H., Verrier, R.L., 1991. Dynamic tracking of cardiac vulnerability by complex demodulation of the T wave. Science 252:437-440.

Nearing, B.D., Verrier, R.L., 2002. Progressive increases in complexity of T-wave oscillations herald ischemia-induced ventricular fibrillation. Circ. Res. 91:727-732.

Nearing, B.D., Verrier, R.L., 2003. Tracking cardiac electrical instability by computing interlead heterogeneity of T-wave morphology. J. Appl. Physiol. 95:2265-2272.

Qu, Z., Shiferaw, Y., Weiss, J.N., 2007. Nonlinear dynamics of cardiac excitation-contraction coupling: An iterated map study. Phys. Rev. E 75:011927.

Ritzenberg, A.L., Adam, D.R., Cohen, R.J., 1984. Period multupling — evidence for nonlinear behaviour of the canine heart. Nature 307:159-161.

Savino, G.V., Romanelli, L., González, D.L., Piro, O., Valentinuzzi, M.E., 1989. Evidence for chaotic behavior in driven ventricles. Biophys. J. 56:273-280.

Shaw, R.M., Rudy, Y., 1997. Electrophysiologic effects of acute myocardial ischemia. A mechanistic investigation of action potential conduction and conduction failure. Circ. Res. 80:124-138.

Singer, D., 1978. Stable orbits and bifurcation of maps of the interval. SIAM J. Appl. Math. 35:260-267.

Strain, M.C., Greenside, H.S., 1998. Size-dependent transition to high-dimensional chaotic dynamics in a two-dimensional excitable medium. Phys. Rev. Lett. 80:2306-2309.

Tachibana, H., Kubota, I., Yamaki, M., Watanabe, T., Tomoike, H., 1998. Discordant S-T alternans contributes to formation of reentry: a possible mechanism of reperfusion arrhythmia. Am. J. Physiol. Heart Circ. Physiol. 275:H116-H121.

Vinet, A., Roberge, F.A., 1994. Analysis of an iterative difference equation model of the cardiac cell membrane. J. Theor. Biol. 170:201-214.

Watanabe, Y., Dreifus, L.S., 1972. Levels of concealment in second degree and advanced second degree A-V block. Am. Heart J. 84:330-347.

Wit, A. L., Janse, M. J., 1993. The Ventricular Arrhythmias of Ischemia and Infarction. Electrophysiological Mechanisms. Futura, Mount Kisco.

Yehia, A.R., Jeandupeux, D., Alonso, F., Guevara, M.R., 1999. Hysteresis and bistability in the direct transition from 1:1 to 2:1 rhythm in periodically driven single ventricular cells. Chaos 9:916-931.

Yehia, A.R., Shrier, A., Lo, K.C.-L., Guevara, M.R., 1997. Transient outward current contributes to Wenckebach-like rhythms in isolated rabbit ventricular cells. Am. J. Physiol. Heart Circ. Physiol. 273:H1-H11.

SUPPLEMENTARY MATERIAL III ("MOVIES OF PROPAGATION")

A. López *et al.*:

"Rhythms of high-grade block in an ionic model of a strand of regionally ischemic ventricular muscle"

These movies show propagation down the one-dimensional cable at the indicated external potassium concentration at three different lengths of the ischemic segment (L = 0.5 cm, 1.0 cm, and 2.0 cm). Each frame of the movie is a snapshot of the membrane voltage (mV) plotted against distance (cm). Propagation is from left to right, and the time between individual frames is 10 ms. Each movie loops, repeatedly showing the same one cycle of each periodic rhythm. The movies are in QuickTime (.mov) format (the QuickTime movie player can be downloaded from www.apple.com/quicktime). The figure numbers in the listing below refer to the figures in the main text of the article.

Length of Ischemic Segment = 1 cm

Figure No.	Rhythm	$[K^+]_o$ (mM)	Supplementary Materials
Fig. 1A-C	1:1	5.4	A
Fig. 1D-F	1:1	13.0	B
Fig. 2A-C	2:2	13.173	C
Fig. 2D-F	2:1	13.250	D
Fig. 3A-C	4:2	13.437	E
Fig. 3D-F	4:1	13.442	F
Fig. 4A-C	6:2	13.472	G
Fig. 4D-F	6:1	13.476	H
Fig. 5A-C	8:2	13.4855	I
Fig. 5D-F	8:1	13.487	J
Fig. 6A-C	2:0	13.494	K
Fig. 6D-F	1:0	13.745	L

Length of Ischemic Segment = 0.5 cm

Figure No.	Rhythm	$[K^+]_o$ (mM)	Supplementary Materials
Fig. 9A-C	2:1	13.571	M
Fig. 9D-F	3:1	13.574	N

Length of Ischemic Segment = 2.0 cm

Figure No.	Rhythm	$[K^+]_o$ (mM)	Supplementary Materials
none	4:1	13.45	O
none	8:2	13.46	P
none	4:1	13.47	Q